APPLICATION OF ADAPTIVE MATERIALS IN FLUTTER SUPPRESSION OF AIRCRAFT STRUCTURES

CONTRACT No. SPC-98-4082

Submitted by

Prof. Afzal Suleman
Instituto Superior Técnico
Departamento de Engenharia Mecânica
Av. Rovisco Pais
1096 Lisboa Codex
PORTUGAL
Tel: 351-1-841 7324
Fax: 351-1-847 4045
E-mail: suleman@ist.utl.pt

FINAL REPORT

October 1998 – October 1999

REPORT DOCUMENTATION PAGE

Form Approved OMB No. 0704-0188

1. AGENCY USE ONLY (Leave blank)	2. REPORT DATE	3. REPORT TYPE AND DATES COVERED
	October 1999	Final Report

4. TITLE AND SUBTITLE

Application of Adaptive Materials for Flutter Suppression in Aircraft Structures

5. FUNDING NUMBERS

F61775-98-WE125

6. AUTHOR(S)

Dr. Afzal Suleman

7. PERFORMING ORGANIZATION NAME(S) AND ADDRESS(ES)

Instituto Superior Tecnico
Departmento de Engenharia Mecanica
Av. Rovisco Pais, 1
Lisbon 1096
Portugal

8. PERFORMING ORGANIZATION REPORT NUMBER

N/A

9. SPONSORING/MONITORING AGENCY NAME(S) AND ADDRESS(ES)

EOARD
PSC 802 BOX 14
FPO 09499-0200

10. SPONSORING/MONITORING AGENCY REPORT NUMBER

SPC 98-4082

11. SUPPLEMENTARY NOTES

12a. DISTRIBUTION/AVAILABILITY STATEMENT

Approved for public release; distribution is unlimited.

12b. DISTRIBUTION CODE

A

13. ABSTRACT (Maximum 200 words)

This report results from a contract tasking Instituto Superior Tecnico as follows: The contractor will investigate the application of integrated adaptive actuators to the problem of flutter control in aircraft structures. The research will focus on electro-mechanical finite element models (FEM) their application to simulations of flutter on airframe components.

14. SUBJECT TERMS

EOARD, Structural Dynamics, Structural Materials

15. NUMBER OF PAGES

61

16. PRICE CODE

N/A

17. SECURITY CLASSIFICATION OF REPORT	18. SECURITY CLASSIFICATION OF THIS PAGE	19, SECURITY CLASSIFICATION OF ABSTRACT	20. LIMITATION OF ABSTRACT
UNCLASSIFIED	UNCLASSIFIED	UNCLASSIFIED	UL

EXECUTIVE SUMMARY

In recent years, vigorous research in materials science has resulted in the development of multifunctional materials. These mechano-electro-magneto-thermo-rheologogical materials when embedded in adaptive composite systems have presented an exceptional promise in the fields of active vibration suppression, shape control and noise attenuation. For deformation of thin structural elements, the most widely used multifunctional materials are piezoelectric actuators. Piezoelectrics have higher bandwidths than are possible in shape memory alloys, they are more compact than magnetostrictive devices and they are bidirectional by nature unlike electrostrictive materials. Design problems in aircraft structures requiring active solutions using adaptive composites to suppress vibration and control the shape of the structure are presented.

Panel flutter is a self-excited oscillating phenomenon and involves interactions between elastic, inertia and aerodynamic forces. When a flight vehicle travels at high supersonic speeds, it may experience nonlinear limit cycle oscillations due to the dynamic pressure and high aerodynamic heating temperature gradients. In order to investigate the performance of active materials in panel flutter suppression, coupled electro-thermo-mechanical nonlinear panel flutter equations of motion are derived using the finite element method. Models for adaptive composite shallow shells with embedded piezoelectric actuators and sensors are developed. Passive and active flutter suppression of adaptive composite aircraft skin panels are presented. Boundary conditions, in-plane forces and shell curvature effects are studied. The results reveal that active flutter control using piezoelectric bending control actions is feasible.

Experimental subsonic aeroelastic flutter and buffeting suppression using piezoceramic actuators and sensors to impart changes in damping and aerodynamic characteristics to the wing have also been investigated. An appreciable buffeting reduction was obtained, especially when using airfoil shape control, which combined with the root actuators were able to decrease the average amplitude in buffeting from 32% to 47.5%. The airfoil shape control also decreased the frequency of the vibration by 34%. To resolve the diminishing control authority of the piezoceramic actuators as air speed is increased, the airfoil shape control has presented a feasible solution where the piezo actuators are used to create a favourable variation in lift characteristics.

ACKNOWLEDGEMENTS

The European Office of Aerospace Research and Development (EOARD) under Contract No. SPC-98-4082 has supported the current investigation. This investigation was accompanied and monitored by Dr. V.B. Venkayya, at the Air Force Research Laboratory, Wright-Patterson AFB and Major Jerry Sellers at EOARD.

TABLE OF CONTENTS

CHAPTER 1

ADAPTIVE STRUCTURES TECHNOLOGY

In the past decade, technological developments in materials and computer sciences have evolved to the point where their synergistic combination have culminated in a new field of multi-disciplinary research in adaptation. The advances in material sciences have provided a comprehensive and theoretical framework for implementing multifunctionality into materials, and the development of high speed digital computers has permitted the transformation of that framework into methodologies for practical design and production. The concept is elementary: a highly integrated sensor system provides data on the structures environment to a processing and control system which in turn signals integrated actuators to modify the structural properties in an appropriate fashion.

The multifunctional mechano-electro-magneto-thermo-rheological materials embedded in adaptive composite systems have presented an exceptional promise in engineering design problems requiring solutions in active vibration suppression, shape control and noise attenuation. Piezoelectric materials, shape memory alloys and magnetostrictive materials are the three most recognized types. These materials develop strains or displacements when exposed to electric, thermal and magnetic fields, respectively.

Actuation Technology

When the **shape memory** alloy is heated above a critical temperature the material recovers its original pre-deformed shape. The most common commercially available shape memory alloy is Nitinol. This alloy is very ductile and can be deformed easily. In addition, it also has good strength and strain rate, it is corrosion resistant, and it is stable at high temperature. A limited number of efforts aimed at using shape memory alloys as actuators in composite structures have been made. Recent studies include the work by Boyd and Lagoudas [1] where they have developed a micromechanical model for shape memory composites, and Sullivan [2], who has developed a model to predict shape memory composite behaviour. Other significant theoretical

studies on the modeling of systems containing shape memory alloys include the works by Liang and Rogers [3], Feng and Li [4] and Graesser and Cozzarelli [5]. Research on using shape memory alloys in active structural control include the works by Baz et al [6], Ikegami et al [7] and Maclean et al [8].

Magnetostrictive materials exhibit a change in dimension when placed in a magnetic field. Terfenol-D is the most popular commercially available magnetostrictive material. Recent research on magnetostrictive materials shows that they provide strokes significantly larger than their electromechanical counterparts however they tend to be difficult to implement in structural systems [9]. Work on composites incorporating magnetostrictive materials include the unimorphs by Honda et al [10] and the micro-composite systems by Bi and Anjanappa [11].

Piezoelectric materials present two distinct characteristics: the 'direct' piezoelectric effect occurs when a piezoelectric material becomes electrically charged when subjected to a mechanical stress. Thus, these devices can be used to detect strain, movement, force, pressure or vibration by developing appropriate electrical responses. The 'converse' piezoelectric effect occurs when the piezoelectric material becomes strained when placed in an electric field. The ability to induce strain can be used to generate a movement, force, pressure, or vibration through the application of a suitable electric field. The most popular commercial piezoelectric materials are lead zirconate titanate (PZT) and polyvinylidene fluoride (PVDF). The potential of applying piezoelectric materials as distributed actuators in composite structures has resulted in several significant studies. Suleman and Venkayya [12] have modelled a simple composite plate structure with piezoelectric layers using classical lamination theory, however, the first reported studies on adaptive composites include the works by Bailey and Hubbard [13], Crawley and de Luis [14], Leibowitz and Vinson [15] and Wang and Rogers [16].

The **electrostrictive** phenomenon is a nonlinear property which exists in all dielectric materials. When an electric field is applied across an electrostrictive material, the positive and negative ions are displaced and a strain is induced in that material. The resulting strain is proportional to the square of the applied electric field and independent of the applied electric field's polarity. Since the strain is proportional to the square of the electric field, the strain will always be

positive. This is analogous with the magnetostrictive behavior described earlier. The most popular electrostrictive material is lead magnesium niobate (PMN); however, this material is still not widely available on the commercial market. These materials generally offer higher electrically induced strain with lower hysteresis than the piezoelectric materials, however constitutive models for electristrictors are not as mature as models for piezoelectrics due to the nonlinearities. Hom and Shankar [17] have formulated a fully coupled constitutive model for electrostrictive ceramic materials. Electrostrictive materials used as distributed actuator elements in adaptive composites have not been reported in the literature.

Magneto- and electro-rheological fluids are multiphase materials consisting of a dispersion of polarizable particles in a carrier oil, and they exhibit properties of a typical viscoelastic material. The utilization of electro-rheological materials for vibration damping has been the subject of considerable research since these materials exhibit fast, reversible and controllable changes in behaviour. However, in spite of advances in sensing and controls, fundamental rheological research as applied to vibration damping has lagged behind. Specifically, essential information in terms of material based structure reliability and controllability is still needed to successfully implement such systems.

Typically, the performance of an actuator is evaluated in terms of the following characteristics: displacement (the ability of the actuator to displace an object; force generation (the amount of force the actuator can produce); hysteresis (the degree of reproducibility in positioning operations); response time (how quickly an actuator can start the actuation process); bandwidth (range of frequencies in which the actuator can operate effectively; temperature range of operation; repeatability and precision of the actuator; power required to drive the actuator; mass of actuator material required for a given displacement; and cost. Table 1 presents the general characteristics of commercially available actuators [18].

The piezoelectric PZT provides the potential for the greatest force handling capability. PZT also operates with the highest bandwidth of the micro actuators and among the highest displacements. Electrostrictive PMN possesses the lowest hysteresis of any of the actuator materials.

Table 1 – Actuator Technology Assessment

	NITINOL	TERFENOL-D	PZT-BM500
Energy	Heat	Magnetic field	Electrical Field
Hysteresis	high	low	low
Bandwidth	Low	moderate	high
Accuracy	poor	high	high
Response time	low	fast	very fast
Power use	high	moderate	moderate
Maturity	new	new	established

However, the temperature operating limits for PMN would require that it be specially insulated. Although PZT is a preferred material for most applications, future commercial applications may favor a direct replacement of PZT with PMN because of its superior hysteresis efficiency.

The shape memory material Nitinol produces the greatest displacements, but the weakest force of the actuators under consideration. This material is very ductile and consequently does not support as much force as the other actuator materials. However, it does give it the advantage of being easily shaped into different actuator geometry. It is less desirable from the point of view of precision and economy of design due to its power consumption, accuracy and hysteresis characteristics. It can also be observed that Terfenol-D and PZT compare very closely in these general characteristics. For deformation of thin structural elements, the most widely used multifunctional materials to date have been piezoelectric actuators. Piezoelectrics have higher bandwidths than are possible in shape memory alloys, they are more compact than magnetostrictive devices and they are bidirectional by nature unlike electrostrictive materials.

Sensing Technology

Optical fibers make excellent strain sensors because they are immune to electromagnetic interference. Optical fibers can be bonded to the surface of a structure or embedded directly into the structure. There are many types of optical fiber sensors. The more useful fiber optic based strain sensors uses the intrinsic properties of the optical fiber. In an intrinsic fiber measurement, one or more of the optical field parameters, which include frequency, wavelength, phase, mode index, polarization, index of refraction and attenuation coefficient, are effected by the environment.

Piezoelectrics sensors tend to operate best in dynamic situations because the induced charge imbalances created by straining the material dissipate with time. How quickly this occurs depends on the materials capacitance, resistivity and output loading. Force transducers utilize piezoelectric elements to produce an electrical output which is proportional to the applied force. The force transducer is mounted in series with the force transmission path in order to directly expose the piezoelectric element to the forces which are to be measured. Since the piezoelectric is preloaded, the force sensor can measure both tensile and compressive forces. A high stiffness ensures a high resonant frequency and it will have a minimum effect on the structural integrity.

In the case of sensors, the technologies considered for the adaptive composites must be able to withstand the composite manufacture process. Embedding issues make Nitinol a questionable choice. If the shape memory alloy had to be electrically insulated from the conductive composite it would complicate the composite manufacturing process and increase the cost significantly.

The performance of any sensor can be evaluated in terms of sensitivity (amount of signal which a sensor will produce for a given change in the variable); the length over which the measurement is made; bandwidth (the frequency range over which the sensor remains effective); response time (the speed at which the sensor can respond to a change in the variable); the temperature range over which the sensor can operate; repeatability and precision of the actuator; weight and cost. Table 2 presents a relative assessment of the sensor types considered suitable for embedding in adaptive composite systems.

Table 2 – Sensor Technology Assessment

	FIBER OPTICS	PZT
Sensitivity	moderate	moderate
Gage Length	moderate	high
Bandwidth	high	moderate
Resolution	high	moderate
Temperature Range	high	high

The temperature range is critical to the adaptive composite system because it is anticipated that the sensors may be embedded and would therefore undergo the composite curing process. Embedding would be feasible in the case of fiber optic sensors, but not as desirable in the case of PZT strain sensors. From an assembly and handling point of view, strain gauges or even PZT are favored because of the availability of knowledge and experience with these techniques.

CHAPTER 2

NONLINEAR PANEL FLUTTER

Panel flutter is a self-excited oscillating phenomenon and involves interactions between elastic, inertia and aerodynamic forces. It is a supersonic/hypersonic aeroelastic phenomenon that is often encountered in the operation of aircraft and missiles. The air flows on one side of the panel. Because of the large deflection geometrical structural nonlinearity, limit cycle oscillations will occur beyond the critical dynamic pressure. When a flight vehicle travels at high supersonic speeds, it will experience flutter due to the dynamic pressure and high temperature owing to the aerodynamic heating. The presence of high temperature load results in a flutter motion at lower dynamic pressures. In addition, the temperature rise may also cause large aerodynamic-thermal deflections of the skin panels, which affect flutter response and can lead to chaotic motion. The mode of failure for panel flutter is fatigue due to limit-cycle oscillations. To increase the critical dynamic pressure or to suppress the limit-cycle oscillations is, therefore, one of the many important factors that an aircraft designer should consider.

Although there has been a voluminous theoretical literature on the panel flutter problem over the past 30 years, most analysis fall into one of the four categories based on the structural and aerodynamic theories employed:

- Linear structural theory; quasi-steady aerodynamic theory
- Linear structural theory; full linearized (inviscid, potential) aerodynamic theory
- Nonlinear structural theory; quasi-steady aerodynamic theory
- Non-linear structural theory; full linearized (inviscid, potential) aerodynamic theory

Of these four solution methods, the linear structural/quasi-steady aerodynamic approach comprises the great bulk of the literature due to its simplicity. Unfortunately, this approach does not account for structural nonlinearities, therefore it can only determine the flutter boundary and give no information about the flutter oscillation itself. Furthermore, the use of the quasi-steady

aerodynamics neglects the three-dimensionality and unsteadiness of the flow; hence it cannot be used in the transonic flight regime. A nonlinear structural/inviscid potential theories represent the state of the art in panel flutter analysis.

A number of classical analytic methods exist for the investigation of limit cycle oscillations of panels in supersonic flow. In general, Galerkin's method is used in the spatial domain, where the panel deflection is expressed in terms of two to six or more linear modes; and various techniques in the temporal domain such as the numerical integration, harmonic balance, and perturbation methods, to cite a few, are employed. All of the analytical investigations have been limited to 2- to 3-dimensional rectangular plates with all four edges simply supported or clamped. The classic approaches also indicate that at least six linear linear normal modes are required for a converged limit-cycle amplitude.

Early works on panel flutter were concerned mainly with conventional isotropic panels. The research progress and some of the references can be found, for example, in the textbooks by Fung [19], Bisplinghoff and Ashley [20], and Dowell [21]. Olson [22], Sander et al [23], Yang and Sung [24], and Mei [25], among others, have studied the flutter of isotropic flat panels using the finite element method. Some studies were also devoted to the flutter of composite panels. For example, Pidaparti and Yang [26] considered the effects of boundary conditions and fiber angle of panels on the flutter boundaries. Rosettos and Tong [27] applied a hybrid stress finite element method and used linearized piston theory to analyze the flutter of anisotropic cantilever plates. Their results indicate that flutter characteristics are strongly dependent on the composite fiber angle and anisotropy. Srinivasan and Babu [28] studied the panel flutter of cross-ply laminated composites by using the integral equations method. Lin et al [29] used an 18 dof high precision triangular finite element to perform a flutter analysis of symmetrically laminated composite panels. Their studies included the effects of composite fiber angle, orthotropic modulus ratio, flow direction, and aerodynamic damping on the flutter boundaries. Sawyer [30] used the Galerkin method to study both the flutter and buckling problems of general laminated plates with simply supported boundary conditions. Oyibo [31] presented an analytical approach by combining classical plate theory and Ackeret's aerodynamic strip theory to study the flutter behaviour of an orthotropic panel. Lee and Cho [32] and Liaw [33] have investigated the use of

composite panels in flutter problems. Lee and Lee [34] have performed supersonic flutter analysis of anisotropic panels taking into consideration the effects of panel geometry, boundary conditions, lamination scheme, flow directions and thermal effects.

Extension of the finite element methods to study nonlinear supersonic/hypersonic limit cycle oscillation of two-dimensional isotropic panels were given by Zhou et al [35], Rao and Rao [36], Sarma and Varadan [37], and Gray and Mei [38]; three dimensional isotropic panels by Mei and Weidman [39], Mei and Yang [40], and Han and Yang [41]; and laminated composite panels by Dixon and Mei [42] and Liaw and Yang [43].

In most of the classic and finite element nonlinear panel flutter studies, the effects of uniform temperature change are treated by an equivalent system of mechanical loads. Few linear panel flutter studies have dealt with temperature distributions directly. Reported studies include the paper by Liaw [44] and Xue and Mei [45] have extended the finite element method to investigate the nonlinear flutter responses of two-dimensional panels with temperature distribution. The thermal environment can affect panel motions by introducing thermal in-plane forces and bending moments.

In panel flutter suppression design problems, the conventional design approach has been to increase the panel stiffness resulting in additional weight With the advent of multifunctional materials and adaptive structures technology, there is been considerable effort reported in the literature investigating the application of adaptive materials and structures technology for passive and active control of flexible structures. Relatively few investigations have concentrated on active panel flutter control. Scott and Weishaar [46] and Hajela and Glowasky [47] proposed linear panel flutter control using piezoelectric actuators and sensors. Zhou et al [48] have extended the use of piezoelectric actuators and sensors to include the nonlinear panel flutter. Xue and Mei [49] have recently studied the feasibility of applying shape memory alloys in linear panel suppression.

Proposed Design Methodology

This study presents an optimal control method to suppress the panel limit-cycle oscillations at dynamic pressures greater than the critical value using piezoelectric actuators and sensors. The nonlinear finite element equations of motion are developed based on the nonlinear geometric large deflection theory. A finite element model for an adaptive composite shallow shell is developed subject to aerodynamic and thermal loads.

Two control strategies are employed to assess the performance of the piezoelectric actuators. First, the in-plane passive actuation capability of the piezoelectric patches is measured and its effect on the aerodynamic parameter is quantified. This approach relies on stiffening the structure by applying in-plane loads to the structure due to identical electrical fields to the top and bottom layers of piezoelectrics on the structure. The second approach consists of actively controlling the structure by allowing the piezoelectric patches to actuate in bending. By applying the optimal control theory, bending control actions can be determined based on the linearized equations of motion.

Numerical simulations based on the nonlinear equations of motion are performed to demonstrate the effectiveness of the piezoelectric actuators. The performance of the actuator designs and the maximum flutter-free dynamic pressure are investigated and presented.

CHAPTER 3

ADAPTIVE COMPOSITE MODEL

For the last two decades, there has been an increased research activity in the area of finite element modelling of adaptive composites. The primary interest has been on the analysis of piezoelectrically actuated composites and early investigations were devoted to three-dimensional electromechanical elements. Among the reported studies, Tzou and Tseng [50] have used variational methods to model finite element piezoelectric solids. Ha et al [51] developed an eight-node three-dimensional composite brick finite element for modeling the dynamic and static response of laminated composites containing distributed piezoelectric ceramics subjected to mechanical and electrical loading. The electrical potential is taken as a nodal degree of freedom, leading to an element with four degrees of freedom per node. These models using three-dimensional finite elements can give accurate results by setting computationally expensive refined meshes with acceptable aspect ratios.

Classical plate theories have been proposed for the analysis of rectangular piezoelectric plates (Lee and Moon [52], Crawley and Lazarus [53], Wang and Rogers [54] and Lam et al [55]). Other plate formulations include the work reported by Chandrashekhara and Agarwal [56], who used a finite element formulation based on first-order shear deformation theory for modeling the behavior of laminated composite plates with integrated piezoelectric sensors and actuators. The developed model does not introduce the voltage as an additional degree of freedom. Tzou and Ye [57] presented a laminated quadratic C^0 piezoelastic triangular shell finite element using the layerwise constant shear angle theory which accounts for a constant approximation of the nonlinear cross-sectional warping applied to piezoelectric laminated systems. A model containing an actuator element, an adhesive interface element and an eight-node isoparametric plate element was developed by Lin et al [58]. An analytic solution is also derived and results are compared with the finite element model. Chattopadhyay and Seeley [59] used a finite element model based on a refined higher order theory to analyze piezoelectric materials surface bounded or embedded in composite laminates. The displacement field accounts for transverse shear stresses through the thickness and satisfies the boundary conditions at the free surfaces. Through

numerical examples they shown that the refined theory captures important higher order effects that are not modeled by the classical laminate theory. Recently, models using higher-order theories for piezoelectric laminates can be found in Reddy and Mitchell [60] and Jonnalagadda et al [61], among others.

Very few composite shell elements with electromechanical properties have been reported in the literature. A 4-noded shell element extending the shallow shell shear deformation theory has been proposed, using an equivalent single layer model for a three layer shell [62]. An 8-noded quadrilateral shell element [63] with no electrical degrees of freedom using the 3D-degenerated shell theory has also been proposed, where the piezoelectric effect was treated as an initial strain problem. An axisymmetric 3-node triangular shell element has also been developed to study mooney transducers [64]. A 12-noded degenerated 3D shell element with a layer-wise constant shear angle has been formulated [65]. However, more research is required to understand and quantify the influence of the curvature on the piezoelectric actuators and sensors. Suleman and Venkayya [12] have reported an efficient finite element formulation for vibration control of a laminated composite plate with piezoelectric sensors and actuators. By modelling the plate and the sensor/actuator system with the four noded bilinear Mindlin plate element, the problems associated with the solid element are eliminated and modelling the plate and the sensor/actuator system with the four noded bilinear Mindlin plate element considerably reduces the problem size.

In the present investigation, the simple quadrilateral plate finite element has been extended to include the effect of curvature for the analysis of adaptive laminated composite shallow shells. The finite element is quadrilateral in shape and has eight nodal points with 40 degrees of freedom.

The objective is to actively control flutter using adaptive shape and vibration control of aircraft skin composite panels with embedded piezoelectric actuators and sensors. Figure 1 shows the adaptive composite configuration and the direction of polarization of the piezoelectric laminates that may comprise a typical wing or fuselage skin panel.

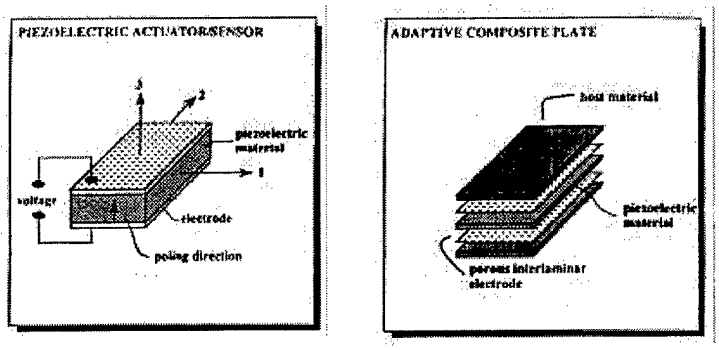

Figure 1 – Adaptive composite configuration and the direction of polarization of the piezoelectric laminates

The formulation and implementation of a structural analysis program to study flutter suppression of curved panels using adaptive composite shallow panels is presented next. Shallow shells are surfaces with negligible curvature compared to its span. The median surface is defined by the radius of curvature R_x and R_y and the twist radius R_{xy}, all assumed constant.

Equations of Motion

To derive the equations of motion for the laminated composite plate, in an aerodynamic field with piezoelectrically coupled electromechanical properties, we use the generalized form of Hamilton's principle

$$\delta \int_{t_1}^{t_2} [T - \Pi + W_e - W_m + W_a]\, dt = 0 \qquad (1)$$

where T is the kinetic energy, Π is the potential energy, W_m is the work done by the magnetic field, W_e is the work done by the electrical field and W_a is the work done by the aerodynamic forces. The kinetic and potential energies can be written in the form

$$T = \int_V \frac{1}{2} \rho\, \dot{\bar{u}}^T\, \dot{\bar{u}}\, dV; \qquad \Pi = \int_V \frac{1}{2} \bar{S}^{c^T}\, \bar{T}^c\, dV$$

where $\overline{S}^c$ and $\overline{T}^c$ are the generalized elastic strain and stress vectors. The work done by the electrical forces can be written as

$$W_e = \int_{V_p} \frac{1}{2} \overline{S}^{e^T} \overline{T}^e \, dV_p$$

where $\overline{S}^e$ is a vector of electrical field (volts/meter) in the piezoelectric material, and $\overline{T}^e$ is a vector of electrical displacements (charge/area). In the context of the present analysis, it is assumed that the work dome by the electromagnetic forces is negligible.

Electromechanical Constitutive Relations

For piezoelectrics the properties are defined relative to the local poling direction. Available piezoelectric materials have the direction of poling associated with the transverse direction and the material is approximately isotropic in the other two directions. In matrix form the equations governing these material properties can be written as

$$\overline{T}^e = \mathbf{e}^T \overline{S}^c + \varepsilon \overline{S}^e$$
$$\overline{T}^c = \mathbf{c} \overline{S}^c - \mathbf{e} \overline{S}^e$$

where $\overline{T}^e$ is the electric displacement vector; $\mathbf{e}$ is the dielectric permittivity matrix; $\overline{S}^c$ is the elastic strain vector; ε is the dielectric matrix at constant mechanical strain; $\overline{S}^e$ is the electric field vector; $\overline{T}^c$ is the elastic stress vector and $\mathbf{c}$ is the matrix of elastic coefficients at constant electric field strength.

Stress-Strain Relations

The composite laminate shell is presumed to consist of perfectly bonded laminae. Moreover, the bonds are presumed to be infinitesimally thin. Thus, following the classical lamination theory, the state of stress in the element is given by

$$\begin{aligned}\overline{S} &= \left\{\overline{T}^m \quad \overline{T}^b \quad \overline{T}^{ts} \quad \overline{T}^e\right\} \\ &= \left\{T_x^m \quad T_y^m \quad T_{xy}^m \quad T_x^b \quad T_y^b \quad T_{xy}^b \quad T_{xz}^{ts} \quad T_{yz}^{ts} \quad D_1 \quad \ldots \quad D_{n_p}\right\}\end{aligned}$$

Eight generalized strains and one electrical field parameter per lamina describe the state of deformation for a Mindlin shell with electromechanical properties. Thus, the augmented generalized strain vector takes the form

$$\begin{aligned}\overline{S} &= \left\{\overline{S}^m \quad \overline{S}^b \quad \overline{S}^{ts} \quad \overline{S}^e\right\} \\ &= \left\{S_x^m \quad S_y^m \quad S_{xy}^m \quad S_x^b \quad S_y^b \quad S_{xy}^b \quad S_{xz}^{ts} \quad S_{yz}^{ts} \quad -E_1 \quad \ldots \quad -E_{n_p}\right\}\end{aligned}$$

The stress-strain relationship takes the form

$$\overline{T} = \begin{Bmatrix}\overline{T}^c \\ \overline{T}^e\end{Bmatrix} = \begin{bmatrix}\mathbf{c} & \mathbf{c} & \mathbf{0} & \mathbf{e} \\ \mathbf{c} & \mathbf{c} & \mathbf{0} & \mathbf{e} \\ \mathbf{0} & \mathbf{0} & \mathbf{g} & \mathbf{0} \\ \mathbf{e}^T & \mathbf{e}^T & \mathbf{0} & \varepsilon\end{bmatrix}\begin{Bmatrix}\overline{S}^m \\ \overline{S}^b \\ \overline{S}^{ts} \\ \overline{S}^e\end{Bmatrix} - \begin{Bmatrix}\overline{\alpha}^m \\ 0 \\ 0 \\ 0\end{Bmatrix}\Delta T$$

where $\mathbf{c}$ is the transformed moduli matrix for each lamina including the piezoelectric layers. The transverse shear stiffness matrix $\mathbf{g}$ is defined in terms of the transverse strain energy through the thickness. ΔT is the temperature gradient across the laminate and $\overline{\alpha}^m$ are the coefficients of thermal expansion for each lamina.

Strain-Displacement Relations

The large deformation strain displacement relation for a general shell element undergoing both extension and bending at any point through the thickness is the sum of membrane and change of curvature strain components:

$$\bar{S}^b = \begin{Bmatrix} S_x^b \\ S_y^b \\ S_{xy}^b \end{Bmatrix} = \begin{Bmatrix} u_{,x} \\ v_{,y} \\ u_{,y} + v_{,x} \end{Bmatrix} + \frac{1}{2} \begin{Bmatrix} w_{,x}^2 \\ w_{,y}^2 \\ 2w_{,x} w_{,y} \end{Bmatrix} + z \begin{Bmatrix} -w_{,xx} \\ -w_{,yy} \\ -2w_{,xy} \end{Bmatrix}$$

The shape functions used for the 8-noded shallow shell element are:

$$N_i^s = \frac{1}{4}(1+\xi\xi_i)(11+\eta\eta_i)(\xi\xi_i+\eta\eta_i-1) \qquad \text{for} \quad i=1,2,3,4$$

$$N_i^s = \frac{1}{2}(1+\xi\xi_i)(1-\eta^2) \qquad \text{for} \quad i=5,7$$

$$N_i^s = \frac{1}{2}(1+\eta\eta n_i)(1-\xi^2) \qquad \text{for} \quad i=6,8.$$

Similarly to the plate element formulation, there are five degrees of displacement degrees of freedom at each node for the elastic behaviour, and there is one potential degree of freedom per layer for the piezoelectric effect. Thus

$$\bar{q}_i^s = \{u \quad v \quad w \quad \theta_x \quad \theta_y \quad\}_i;$$
$$\bar{q}^e = \{\phi_1 \quad \cdots \quad \phi_{n_p}\}$$

for $i = 1, 2, \ldots, 8$.. The strain-displacement relations are based on the von Karman deformation theory and the electric field-potential relations $\bar{S}^e = -\nabla\phi$. The potential degrees of freedom are constant throughout the plane of the piezoelectric layer and they are assumed to vary linearly through the thickness. Thus the matrix relating the generalized strains to the nodal displacements and electric potentials can be written as follows:

$$\bar{S} = \begin{Bmatrix} \bar{S}^s \\ \bar{S}^e \end{Bmatrix} = \begin{bmatrix} \mathbf{b}^s & \mathbf{0} \\ \mathbf{0} & \mathbf{b}^e \end{bmatrix} \begin{Bmatrix} \bar{q}^s \\ \bar{q}^e \end{Bmatrix}$$

where for the shell element

$$\mathbf{b}_i^s = \begin{bmatrix} \frac{\partial N_i^s}{\partial x} & 0 & -\frac{N_i^s}{R_{xx}} & 0 & 0 \\ 0 & \frac{\partial N_i^s}{\partial y} & -\frac{N_i^s}{R_{yy}} & 0 & 0 \\ \frac{\partial N_i^s}{\partial y} & \frac{\partial N_i^s}{\partial x} & -2\frac{N_i^s}{R_{xy}} & 0 & 0 \\ 0 & 0 & 0 & 0 & z\frac{\partial N_i^s}{\partial x} \\ 0 & 0 & 0 & -z\frac{\partial N_i^s}{\partial y} & 0 \\ 0 & 0 & 0 & -z\frac{\partial N_i^s}{\partial x} & z\frac{\partial N_i^s}{\partial x} \\ 0 & 0 & \frac{\partial N_i^s}{\partial x} & 0 & N_i^s \\ 0 & 0 & \frac{\partial N_i^s}{\partial x} & -N_i^s & 0 \end{bmatrix} \qquad \textit{for} \qquad i = 1, \cdots, n_{el}$$

The element stiffness and mass matrices are first evaluated by expressing the integrals in the local natural coordinates ξ and η of the element and then performing numerical integration using the Gaussian quadrature. The element matrices are then assembled to obtain the global $\mathbf{K}_{ss}$ and $\mathbf{M}_{ss}$ matrices after appropriate transformation to account for the curved nature of the shell surface. Substituting for the generalized stress and strain expressions into Equation (1), we obtain the mass, elastic stiffness and piezoelectric stiffness matrices:

$$\begin{aligned} \mathbf{M}_{cc}^j &= \int_{V_j} \rho\, \mathbf{N}^T \mathbf{N}\, dV_j, \\ \mathbf{K}_{cc}^j &= \int_{V_j} \mathbf{b}^{c^T} \mathbf{c}\, \mathbf{b}^c\, dV_j, \\ \mathbf{K}_{ce}^j &= \int_{V_j} \mathbf{b}^{c^T} \mathbf{e}\, \mathbf{b}^e\, dV_j, \\ \mathbf{K}_{ee}^j &= \int_{V_j} \mathbf{b}^{e^T} \mathbf{e}\, \mathbf{b}^e\, dV_j, \qquad \textit{for} \qquad j = 1, \cdots, n_{el} \end{aligned}$$

Geometric Stiffness

In the passive control methodology adopted in this study, the in plane forces generated by the piezoelectric actuators are accounted for through the nonlinear geometric stiffness matrix. The terms in the geometric stiffness matrix for an element are linear functions of the components of stress in the element. For plate and shell elements it is usual to consider only the membrane stresses. The elements of the geometric stiffness matrix $\mathbf{K}_g$ can be derived from a potential energy function Π_g given by the expression

$$\mathbf{K}_g = \frac{\partial^2 \Pi_g}{\partial x \partial y}$$

where

$$\Pi_g = \frac{1}{2}\iint \left(\chi_1{}^T \mathbf{G}_a \chi_1 + \chi_2{}^T \mathbf{G}_b \chi_2 \right) T \, dS,$$

and

$$\chi_1 = \begin{Bmatrix} -\dfrac{\partial u}{\partial y} \\ \dfrac{\partial v}{\partial x} \\ \dfrac{\partial u}{\partial x} - \dfrac{\partial v}{\partial y} \end{Bmatrix}; \qquad \chi_2 = \begin{Bmatrix} \dfrac{\partial w}{\partial x} \\ \dfrac{\partial w}{\partial y} \end{Bmatrix}; \qquad \mathbf{G}_a = \begin{bmatrix} T_x^m & 0 & -\dfrac{T_{xy}^m}{2} \\ 0 & T_x^m & -\dfrac{T_{xy}^m}{2} \\ -\dfrac{T_{xy}^m}{2} & -\dfrac{T_{xy}^m}{2} & 0 \end{bmatrix}; \qquad \mathbf{G}_b = \begin{bmatrix} T_x^m & T_{xy}^m \\ T_{xy}^m & T_y^m \end{bmatrix}$$

The membrane stress components are initially determined by prescribing a voltage to the piezoelectric patches and subsequently the calculated stresses are used to setup the geometric stiffness matrix.

Aerodynamic Loads

The aerodynamnic theory employed the most for flutter at supersonic flow $\left(M_\infty > \sqrt{2}\right)$ is the quasi-steady, first order piston theory. The aerodynamic pressure can be expressed as

$$p_a = -\frac{2q}{\sqrt{M_\infty^2 - 1}}\left(w_{,x} + \frac{M_\infty^2 - 2}{M_\infty^2 - 1}\frac{1}{V_\infty}w_{,t} - \frac{1}{2r\sqrt{M_\infty^2 - 1}}w_{,t}\right).$$

We can re-write this equation in the following form:

$$p_a = -\left(\lambda\frac{D}{a^3}w_{,x} + \frac{g_a}{\omega_0}\frac{D}{a^4}w_{,t} - \frac{\lambda}{2r\beta}\frac{D}{a^3}w_{,t}\right)$$

where $q = \rho_a V^2/2$ is the dynamic pressure; ρ_a is the air density; V is the airflow speed, M_∞ is the Mach number, a is the panel length, $D = Eh^3/12\left(1-\nu^2\right)$ is the bending rigidity, r is the radius of curvature and $\omega_0 = \left(D/\rho h a^4\right)^{1/2}$ is a convenient reference frequency. The non-dimensional dynamic pressure λ and aerodynamic damping g_a coefficients are given by:

$$\lambda = \frac{2q_a a^3}{D\sqrt{M_\infty^2 - 1}}; \qquad g_a = \sqrt{\lambda\frac{\mu\left(M_\infty^2 - 2\right)^2}{\beta\left(M_\infty^2 - 1\right)}}$$

where $\beta = \sqrt{M_\infty^2 - 1}$, and $\mu = \rho_a a/m_0$ is the air-panel mass ratio and m_0 is the average mass density per unit area of the panel. For high supersonic flows i.e. $\left(M_\infty >> 1\right)$, $g_a \approx \sqrt{\lambda\mu/M_\infty}$.

Thus, the work done by the external aerodynamic forces is given by:

$$W_a = -\int_A \left(\lambda \frac{D}{a^3}\frac{\partial w}{\partial x} + \frac{g_a}{\omega_0}\frac{D}{a^4}\frac{\partial w}{\partial t} - \frac{\lambda}{2r\beta}\frac{D}{a^3}\frac{\partial w}{\partial t} \right) w \, dA$$

Substituting into Equation (1), we obtain the following aerodynamic damping and stiffness matrices for each element:

$$\mathbf{G}^j = \left(g_a - \frac{\lambda}{2r\beta}\frac{D}{a^3} \right) \int_A \mathbf{N}^T \mathbf{N} \, dA,$$

$$\mathbf{K}_a^j = \lambda \int_A \mathbf{N}^T \mathbf{N}_{,x} \, dA \qquad \textit{for} \qquad j = 1, \cdots, n_{el}$$

The aerodynamic stiffness matrix is non-symmetric, due to the non-conservative nature of the aerodynamic loading.

For the entire structure, using the standard assembly technique for the finite element method and applying the appropriate boundary conditions, we obtain the complete equations of motion for a thermo-piezoelectrically coupled electromechanical composite panel in a flow field

$$\overbrace{\begin{bmatrix} \mathbf{M}_{cc} & \mathbf{0} \\ \mathbf{0} & \mathbf{0} \end{bmatrix}}^{inertia} \begin{Bmatrix} \ddot{\overline{U}}^c \\ \ddot{\overline{U}}^e \end{Bmatrix} + \overbrace{\begin{bmatrix} \mathbf{G} & \mathbf{0} \\ \mathbf{0} & \mathbf{0} \end{bmatrix}}^{aero\ damping} \begin{Bmatrix} \dot{\overline{U}}^c \\ \dot{\overline{U}}^e \end{Bmatrix} + \overbrace{\begin{bmatrix} \mathbf{K}_{cc} & \mathbf{0} \\ \mathbf{0} & \mathbf{0} \end{bmatrix}}^{linear\ stiffness} \begin{Bmatrix} \overline{U}^c \\ \overline{U}^e \end{Bmatrix} + \overbrace{\begin{bmatrix} \mathbf{0} & \mathbf{K}_{ce} \\ \mathbf{K}_{ec} & \mathbf{K}_{ee} \end{bmatrix}}^{piezo\ stiffness} \begin{Bmatrix} \overline{U}^c \\ \overline{U}^e \end{Bmatrix} +$$

$$\overbrace{\begin{bmatrix} \mathbf{K}_{\Delta T} & \mathbf{0} \\ \mathbf{0} & \mathbf{0} \end{bmatrix}}^{thermal\ stiffness} \begin{Bmatrix} \overline{U}^c \\ \overline{U}^e \end{Bmatrix} + \overbrace{\begin{bmatrix} \mathbf{K}_a & \mathbf{0} \\ \mathbf{0} & \mathbf{0} \end{bmatrix}}^{aero\ stiffness} \begin{Bmatrix} \overline{U}^c \\ \overline{U}^e \end{Bmatrix} + \overbrace{\begin{bmatrix} \mathbf{K}_g & \mathbf{0} \\ \mathbf{0} & \mathbf{0} \end{bmatrix}}^{nonlinear\ stiffness} \begin{Bmatrix} \overline{U}^c \\ \overline{U}^e \end{Bmatrix} = \begin{Bmatrix} P_{\Delta T} \\ \mathbf{0} \end{Bmatrix}$$

where

$\mathbf{M}_{cc}$ is the mass matrix;

$\mathbf{G}$ is the aerodynamic damping matrix;

$\mathbf{K}_{cc}$ is the linear elastic stiffness matrix

$\mathbf{K}_{ce}$ is the electromechanical coupling matrix;

$\mathbf{K}_{ee}$ is the piezo dielectric matrix;

$\mathbf{K}_{\Delta T}$ is the initial thermal stress stiffness matrix

$\mathbf{K}_{g}$ is the nonlinear stiffness matrix

The equations of motion for a laminated adaptive composite panel with piezoelectric actuators and sensors subjected to aerodynamic and thermal loads have been presented.

Solution Procedure

To solve the nonlinear eigenvalue problem, an iterative procedure is used. For a given set of aerodynamic parameter λ, in-plane force N, mode number, and maximum amplitude, the iteration starts from a corresponding initial mode shape obtained from linear flutter analysis, with amplitude scaled up by a small factor. Based on this initial mode shape, the tangential stiffness matrix $\mathbf{K}_T$ is formed, and an eigenvalue and its corresponding eigenvector are found. This eigenvector is then scaled up again, and the iteration continues until the convergence criterion $|\varphi|$ for k is achieved:

$$|\varphi| = \left|\frac{\Delta k_i}{k_i}\right| \leq 10^{-3}$$

where Δk_i is the change in eigenvalue during the i^{th} iterative cycle. When $\lambda = 0$, the problem is reduced to that of finding the in-vacuo frequencies for the nonlinear vibration of plates. As dynamic pressure λ is increased from zero, two of these eigenvalues will usually approach each other and coalesce to k_{cr} at $\lambda = \lambda_{cr}$ and become a complex conjugate pair for $\lambda > \lambda_{cr}$. Here λ_{cr} is considered to be that value of λ at which the first coalescence occurs for a specific amplitude of the limit cycle oscillation.

CHAPTER 4

FLUTTER ANALYSIS AND CONTROL

To evaluate the present finite element formulation and solution procedure and to study the effects of certain design parameters on the nonlinear supersonic flutter behaviour of adaptive composite panels, a series of simulations for the nonlinear supersonic flutter analysis of adaptive composite panels were performed with the results presented, discussed, and physically interpreted.

A $25\times25\times0.025$ *cm* isotropic square plate (6061-T6 aluminum) was used in all simulations and a 10x10 element mesh was used to obtain the element linear stiffness, initial stress, nonlinear stiffness, mass, and aerodynamic matrices. This grid was shown to numerically to be sufficiently fine and accurate for all the present simulation cases.

A preliminary linear flutter analysis was performed to provide information regarding the airflow speed at which the panel becomes dynamically unstable and the amplitude of oscillation grows with time. As the amplitude increases to a certain level, the nonlinear effects become dominant and the amplitude reaches a bounded value defined by the limit cycle oscillation.

Typical eigenvalue coalescence results obtained by using the finite element method for a simply supported plate are shown in Figure 2. The results were compared with data reported by Mei [25] and it is observed that the present finite element formulation gives accurate results.

Boundary support effect

In Figure 3, the panel amplitude of the limit cycle oscillation is given as a function of λ for simply supported and clamped boundary conditions. The limit cycle oscillations are different since the clamped plate is a much stiffer structure compared to the simply supported boundary conditions.

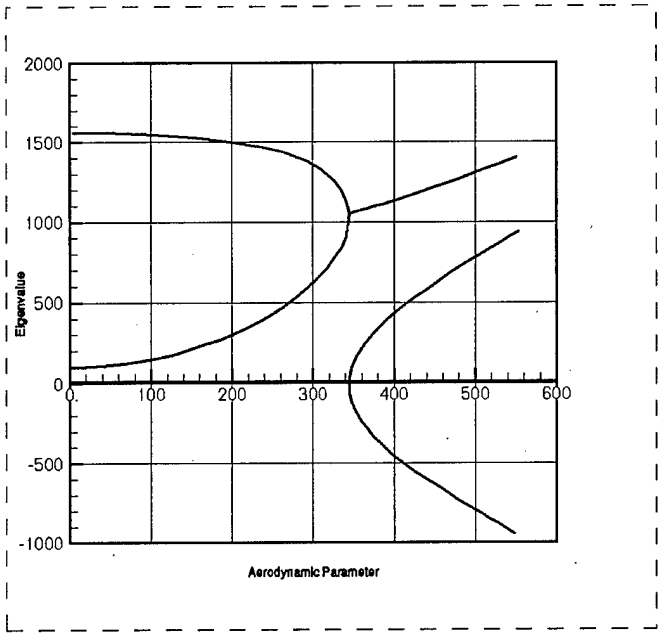

Figure 2 - Typical variation of eigenvalues with dynamic pressure for a simply supported panel

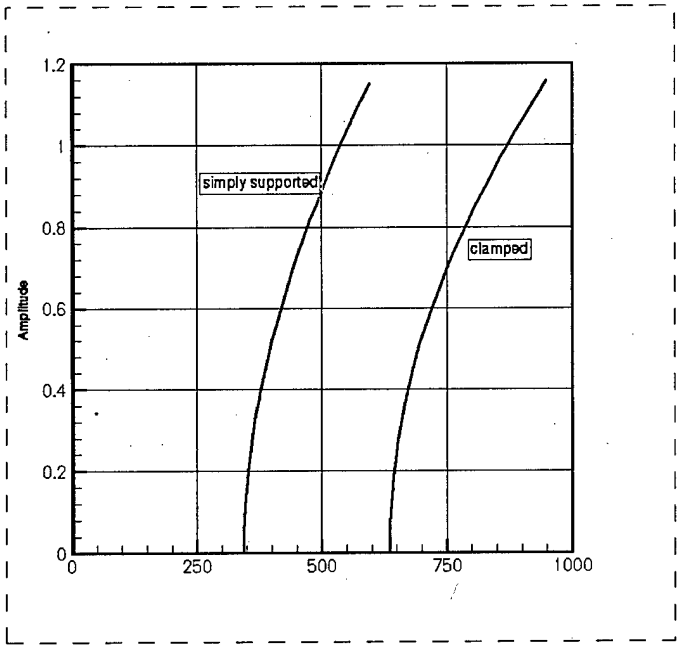

Figure 3 – Limit cycle amplitude vs. dynamic pressure for simply supported panel for two different support conditions

Effect of in-plane loading

Figure 4 shows the panel amplitude vs. aerodynamic parameter for different in-plane forces acting on a simply supported panel. The classical Euler buckling load for simply supported panels is $N_{cr} = -\pi^2 D/a^2$. The total membrane force is composed of the applied in-plane load N_{x0} and the membrane force N_x induced by the large deflections of the panel. It is observed that the applied compressive in-plane force reduces the critical dynamic pressure. However, as the dynamic pressure is increased, the panel amplitude increases, which induces tensile in-plane forces that counteract the applied compressive forces. This process continues until a flutter dynamic pressure is reached which corresponds to a given limit cycle amplitude.

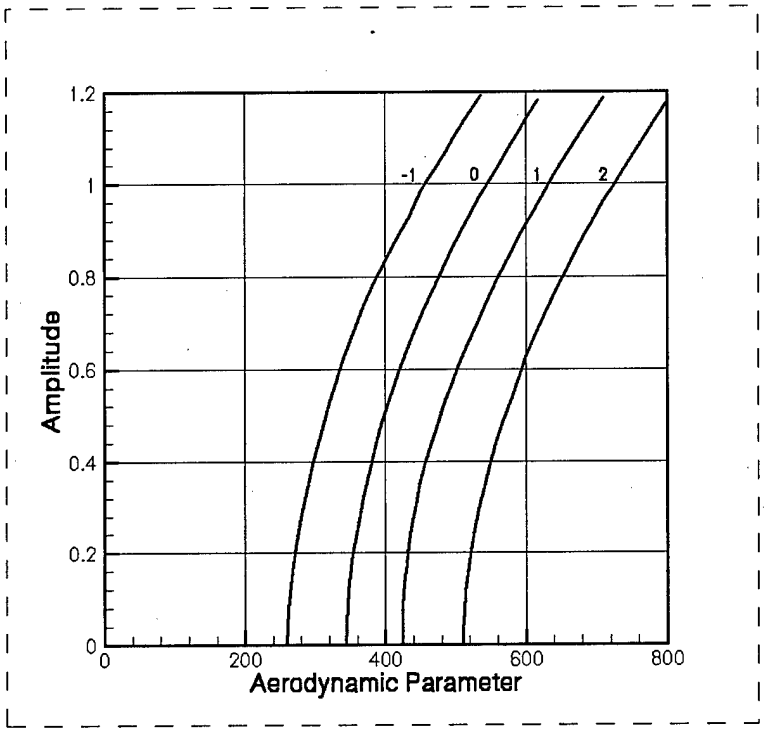

Figure 4 – Limit cycle amplitude vs dynamic pressure for simply supported panel under different in-plane forces

Curved Panels

The application of the present shallow shell finite element formulation in flutter simulation of simply-supported cylindrical and sperical skin panels is shown. The curved panels were assumed to have a radius of curvature $R_x = R_y = 500\,cm$. The coalescence of modes for the cylindrical and spherical panels are shown in Figures 5 (a and b), respectively. It can be observed that for the cylindrical panel, the flutter mode is caused by the coalescence of modes 1 and 3, while for the spherical shells, the critical flutter is caused by the coalescence of modes 1 and 2 for both cases. Summarizing, the curvature has an effect on the coalescence of modes and flutter does not necessarily occur by the coalescence of the two lowest modes.

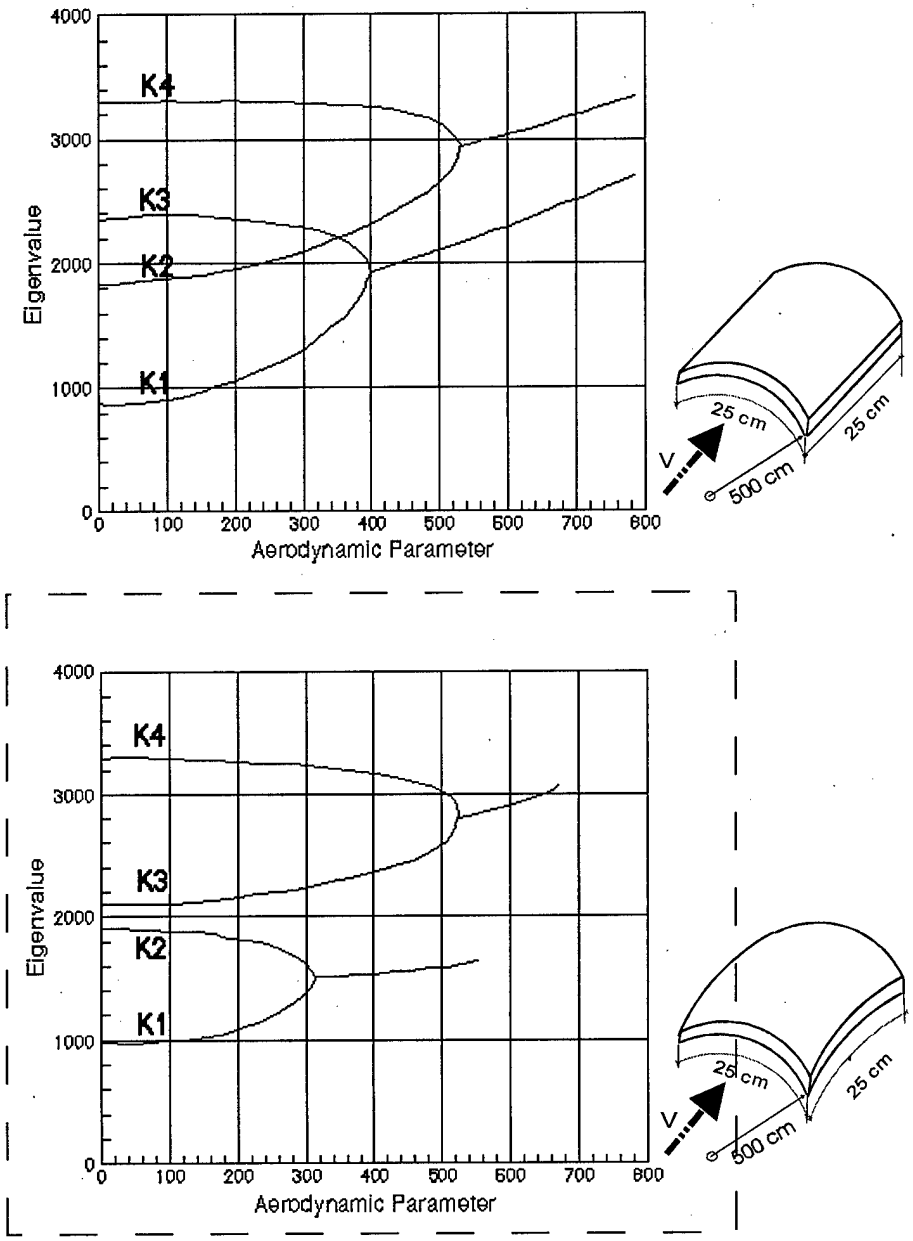

Figure 5 – Coalescence of modes for cylindrically and spherically curved panels with all simply supported edges.

NONLINEAR FLUTTER CONTROL

Passive Control

Before attempting to use piezoelectric materials in panel flutter control problems, a knowledge of the degree of control authority exhibited by a typical piezoelectric actuator needs to be quantified.

Relationships between the applied forces and the resultant responses depend upon the piezoelectric properties of the material, the size and shape of the patch and the direction of the electrical and mechanical excitation. For example, consider a typical piezoceramic patch with dimensions *5 x 5 x 0.05 cm*. The stress free length change in the in-plane direction can be expressed as $D L = d_{31} E a = 6.6$ mm, where *E*, the electrical field, is the applied voltage per unit length. The strain free force in the in-plane direction due to an applied voltage of *400 V* is $F = Y d_{31} E b h = 200 N$.

The effect of in-plane stresses is particularly important since passive control can be implemented by the in-plane stresses generated by the piezoelectric layers in the composite panel. It will be assumed that the panel has reached a state of equilibrium due to the presence of the in-plane stresses, and the stability of the system will be examined at that position. It is also assumed that the panel has not reached a buckled state. The effect of the initial pre-stress gives rise to the geometric stiffness matrix $\mathbf{K_g}$

The question that needs to be raised now is the piezoceramic patch capable of generating a significant force output in order to affect the stiffness of the panel, and thus push back the flutter boundary envelope. Tensile loading, which can be generated by piezoelectric actuators, causes the flutter boundary to shift considerably. For example, for a simply-supported panel with dimensions *30 x 30 x 0.1 cm*, the range of in-plane force that affects the coalescence of the first mode lies in the *200* to *2,000 N* range. It can be inferred that an arrangement of piezoelectric

patches where each exerts an in-plane force of approximately *200 N*, due to an applied voltage of *400 V*, could considerably affect the panel flutter characteristics.

First, let us examine the development of flutter in the panel, in the absence of any piezolectric actuation. The aluminium panel is simply supported along all four of its sides. As the dynamic pressure increases, the natural frequencies of the first and second modes get closer, until they coalesce, and the dynamic pressure λ at this point is called the critical dynamic pressure. For this particular panel, neglecting the aerodynamic damping effect, the critical dynamic pressure parameter is *38.8* psi. After coalescence of the first two modes, the imaginary parts of the eigenvalues become split, one towards the negative side, and the other towards the positive side. When λ passes the critical point, the system becomes inherently unstable, such that a small disturbance makes the amplitude of the panel deflection diverge. As λ increases further, the third and fourth modes coalesce as well.

Using the passive control methodology, the flutter velocity of panels, or similarly the critical dynamic pressure, can be increased by making piezoelectric actuators induce in-plane tensile forces that alter the effective stiffness of the panel. The same voltage is applied to the top and bottom piezoelectric layers, resulting in uniform compression or tension in the plate. This static loading condition on the panel induces in-plane stresses N_x, N_y and N_{xy}. These stresses are subsequently used to calculate the geometric stiffness of the plate, which couples the in-plane and transverse motions of the panel. Subsequently, the geometric stiffness matrix is added to the linear stiffness matrix, and the eigenvalue problem is solved. The value for λ at which a complex solution exists is considered to be the onset of flutter. When the piezoelectric patches create a state of tension in the panel, the dynamic pressure increases. If the piezoelectric patches exert compressive forces on the panel, the dynamic pressure decreases.

Now, let us examine a passive actuation configuration in which the piezoelectric patches cover the center of the plate (Figure 6). First, consider a case where the patches cover only *6%* of the plate area. Here, the mass increases by *17%* due to the addition of the piezo patches to the base structure. Obviously, the effective stiffness also increases. It was observed that the critical dynamic pressure increased from *36.8* to *46.9*, an improvement of *27%*. Note that this increase is

solely due to the bonding of the piezo patches to the top and bottom surfaces of the aluminum panel. Subsequently, the piezo patches were actuated with a voltage of *400 V* and, in this instance, a further increase of *42%* was attained, relative to the case where no voltage was applied. Summarizing, a better performance was indeed attained by the piezoelectric actuation. The effective stiffness was increased by merely attaching the piezo patches in the first instance, and a further increase was obtained by actuating the piezo patches with an applied voltage.

Next, the performance of a patch which covered *25%* of the plate area was assessed. Here, a substantial increase in mass was observed *(69%)*. The addition of piezo patches with no voltage applied resulted in an increase of *92%* in dynamic pressure. Further application of *400 V* across each layer resulted in a smaller further improvement in dynamic pressure to *93.5*, or *32%* relative to the *0 V* case. Thus, it is noted that an increase in size of the piezo patches and/or actuation power, does not necessarily result in better performance. In fact, the *25%* patch configuration performed worse than the *6%* patch case. Apparently, the larger piezo patch configuration resulted in a relatively much larger mass increase thus offsetting the benefits of an increased actuation capability.

Three more patch configurations have been analyzed to further probe this matter. Let us call these configurations 1, 2 and 3, as shown in Figure 6. In configuration 1, five piezo patches are placed in a star shaped form, resulting in a mass increase of *86%*. The flutter dynamic pressure, in the presence of an applied voltage of *400 V*, exhibits a poor performance with a mere *5%* increase in value relative to the no applied voltage case. In other words, a larger actuation capability, followed by a much larger mass increase resulted in a negligible improvement. For configuration 2, with 4 piezoelectric patches arranged in a cross shape, the mass increased by *69 %*. The resultant critical dynamic pressure increased by *8%* to *99.2* due to an applied voltage of *400 V*. Finally, configuration 3 with the piezo patches arranged along the perimeter of a square at the centre of the plate, exhibited an increase of *20%* in dynamic pressure, with an increase of *52%* in mass. Thus, in configuration 3, a better performance was attained in the presence of a relatively smaller increase in mass, while in configuration 1, a poor performance was exhibited with an increase in mass.

Another aspect that draws attention is the fact that the *25%* central patch configuration and the number 2 configuration provide a similar mass increase *(69%)*. However, the *25%* central patch configuration resulted in a *32%* improvement in dynamic pressure, while the actuation in configuration 2 exhibited a poor *8%* improvement. On a preliminary analysis basis, it can be inferred that not only is the added mass to stiffness ratio important, but also the configuration and placement of the patches on the structure should be taken into account during the design process.

Summarizing, there is an optimum patch size, and there in an optimal patch configuration which deliver the best performance. A compromise needs to be found between the advantages of an increased actuation capability and the disadvantages of an increased weight due to the addition of piezoelectric material. These questions need to be addressed through formal optimization design procedures.

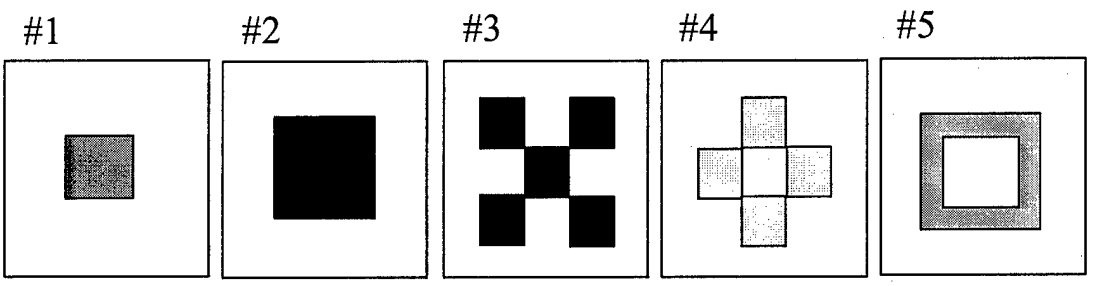

Critical Aerodynamic Parameter $\lambda_{critical}$ = 36 .8					
	Configuration				
	#1	#2	#3	#4	#5
0 V	46.9	70.5	88.5	91.8	63.9
400 V	66.7	93.5	92.5	99.2	76.5
$\lambda_{critical}$	+42%	+32%	+5%	+8%	+20%
Mass	+17%	+69%	+86%	+69%	+52%

Figure 6 – Passive control performance for 5 different piezoelectric patch configurations.

Active control

The bending moment induced by the piezoelectrics s not effective to control the linear panel flutter since there is no bending behaviour in the linear case. On the other hand, the induced in-plane force is not sufficient in linear panel flutter control because of the low modulus and limited ability of the piezoelectrics to create large in-plane forces.

For suppression of panel flutter limit-cycle motions, an optimal control approach based on the linear optimal control theory is proposed. The linear panel flutter is unstable when $\lambda > \lambda_{cr}$, whereas the nonlinear panel flutter is a stable limit-cycle oscillation. Since the flutter is caused by the instability of the linear model, the goal of the control design is to keep the system stable. The active control methodology selected is based on the state-space domain since the system is a multi-input-multi-output with a large number of piezoelectric actuators and sensors. The generic state space equation for a dynamic system is given in the form

$$\dot{\bar{x}} = \mathbf{A}\bar{x} + \mathbf{B}\bar{u} + \mathbf{F}\bar{v}$$
$$\bar{y} = \mathbf{C}\bar{x} + \mathbf{D}\bar{u} + \bar{w}$$

where $\bar{x}$ is the system state vector, $\bar{u}$ is the actuator input vector, $\bar{y}$ is the sensor output vector, $\bar{v}$ is the states perturbation vector, $\bar{w}$ is the sensor noise vector, $\mathbf{A}$ is the system dynamics matrix, $\mathbf{B}$ is actuator input matrix, $\mathbf{C}$ and $\mathbf{D}$ are output modelling matrices and $\mathbf{F}$ is the state perturbation matrix.

A common form of control relies in feeding back the sensed output variables multiplied by a constant matricial factor (gain matrix $\mathbf{G}$). This form of control is known as the linear feedback control, i.e.

$$\bar{u} = -\mathbf{G}\bar{y}$$

The linear Quadratic Regulator (LQR) has been selected to determine the values of the matrix **G**. The LQR method is based on the assumption that all the states of the system are measurable. When it is not possible to measure all the states of the system, there is a need to implement an observer. The observer output is an estimate of the states of the system $\hat{x}$. Thus, the controller is composed of two main blocks: the estimator, which receives the input and output of the system and processes the states of the system; and the feedback gain, which receives the state estimates and processes the system control actuation.

The closed loop dynamics of the system can be represented as follows:

- Plate Structural Model:

$$\dot{\bar{x}} = \mathbf{A}_f \bar{x}_f + \mathbf{B}_f \bar{e}^a + \mathbf{F}_f v$$
$$\bar{e} = \mathbf{C}_f \bar{x}_f + w$$

- Observer dynamics:

$$\dot{\hat{x}}_r = \mathbf{A}_r \hat{x}_r + \mathbf{B}_r \bar{e}^a + \mathbf{K}\left(\bar{\mathbf{e}}^s - \mathbf{C}_r \hat{x}_r\right)$$

- Feedback law

$$\bar{e}^s = -\mathbf{G}\hat{x}_r$$

where the subscript *f* refers to the full state model and *r* refers to the reduced order model. Combining the above equations, the dynamics of the closed loop system can be written in matrix form as:

$$\begin{Bmatrix} \dot{\bar{x}}_f \\ \dot{\hat{x}}_r \end{Bmatrix} = \begin{bmatrix} \mathbf{A}_f & \mathbf{B}_f\mathbf{G} \\ \mathbf{K}\mathbf{C}_f & \mathbf{A}_r - \mathbf{B}_r\mathbf{G} - \mathbf{K}\mathbf{C}_r \end{bmatrix} \begin{Bmatrix} \bar{x}_f \\ \hat{x}_r \end{Bmatrix} + \begin{bmatrix} \mathbf{F}_f & \mathbf{0} \\ \mathbf{0} & \mathbf{F} \end{bmatrix} \begin{Bmatrix} \bar{v} \\ \bar{w} \end{Bmatrix}$$

The numerical simulation was carried out using the MATLAB software tool. The block diagrams for the complete model with feedback is presented in Figure 7. The Kalman observer is a state-space block with matrices $\mathbf{A}_e$, $\mathbf{B}_e$, $\mathbf{C}_e$ and $\mathbf{D}_e$. The inputs for the dynamic model are the actuation

voltages e^a. There are two outputs from the dynamic model block: the states of the system and the sensed voltages from the sensor piezo patches e^u. The state vector is used to compare with the estimated states and the sensed voltages are fed to the observer block.

There is also an error calculation block. The purpose of this block is to calculate the error generated by the observer and this is given by

$$\text{error} = (\bar{x} - \hat{x}) \circ (\bar{x} - \hat{x})$$

The penalty function weight matrices Q and R were defined as diagonal with a value of 10000 and 1×10^{-5}, respectively. The noise covariance for the states was set at 10% of the initial deflection. For the sensor noise, the non-correlated covariance matrix was set with a noise power of 2 V^2. These values were used to design the controller in all simulations. The full order model accounts for all the degrees of freedom included in the plate model while the reduced order model includes only the first 6 modes of vibration. The first 6 natural frequency values for an isotropic square plate with four pairs of actuators and 2 pairs of sensors are shown below:

Mode	ω_n (rad/s)
1	57.30
2	365.47
3	1057.71
4	1133.86
5	1193.71
6	2178.08

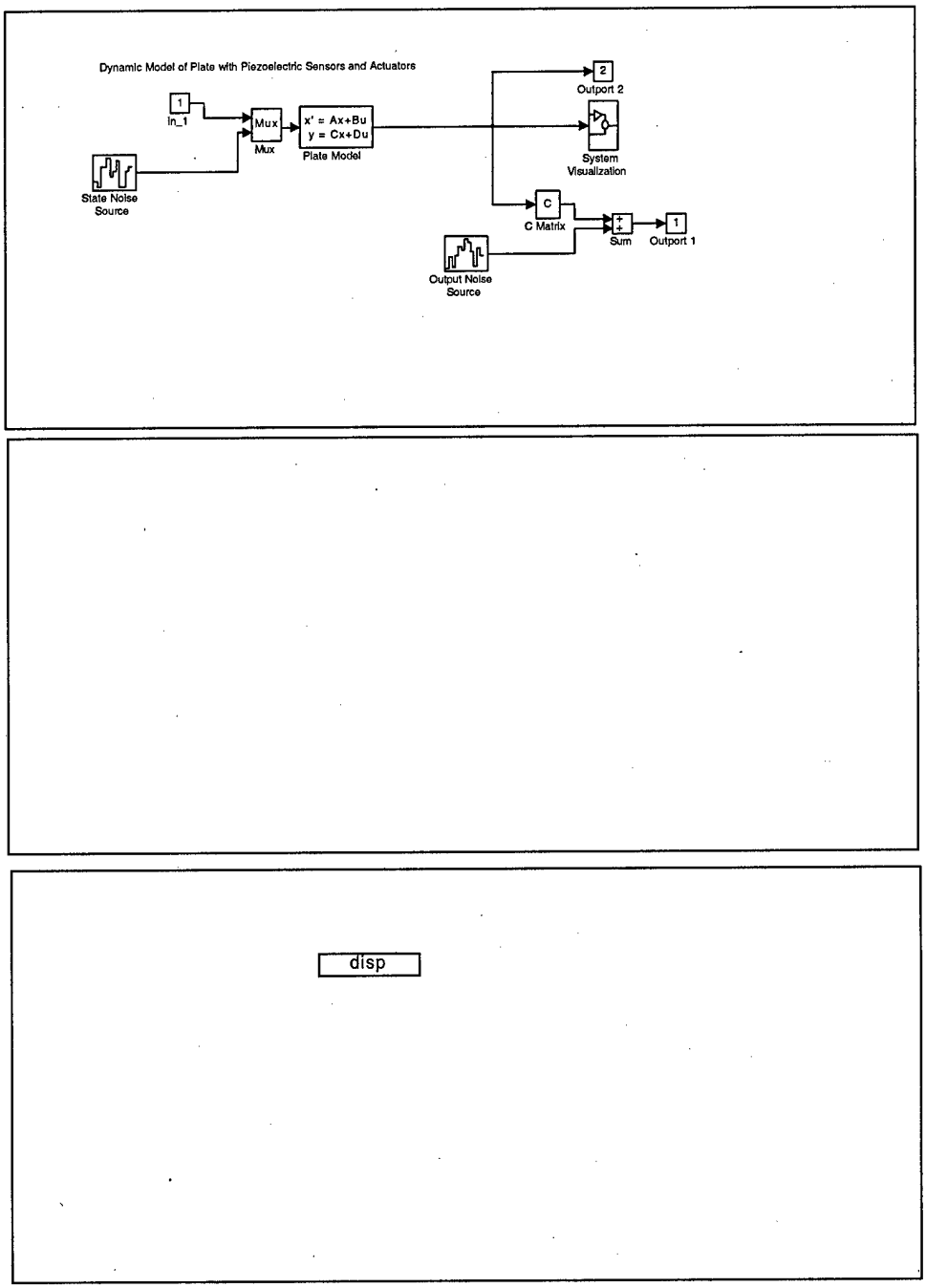

Figure 7 – Block diagram for the complete model with feedback, state observer and error estimation.

The table below depicts the first six modes controlled by a reduced order controller.

Mode	Open Loop	Closed Loop		
	ω_n (rad/s)	ω (rad/s)	Damping	Comments
1	57.30249	57.30438561	0.009520978	Structure
2	365.4731	70.25461695	0.927711305	Controller
3	1057.714	365.4493213	0.007791086	Structure
4	1133.858	567.3243875	0.52316159	Controller
5	1193.705	1056.67806	0.000688374	Structure
6	2178.078	1133.858129	0	Structure

The comments column refers to the origin of the mode that is determined by comparing the natural frequencies of the system in open and closed loop architecture. As can be observed, the controller in the closed loop system introduces two additional modes, which are equivalent to four additional states. From the table, it can also be observed that there are two well behaved modes (2^{nd} and 4^{th}) which are associated with the controller. Also it was observed that the modes estimated by the controller (1^{st} and 3^{rd}) present low damping while the remaining modes present zero damping, which means that the controller does not affect these modes. This indicates the possibility of a spill-over effect. Figure 8 shows time history plots of the 1^{st} and 2^{nd} modes.

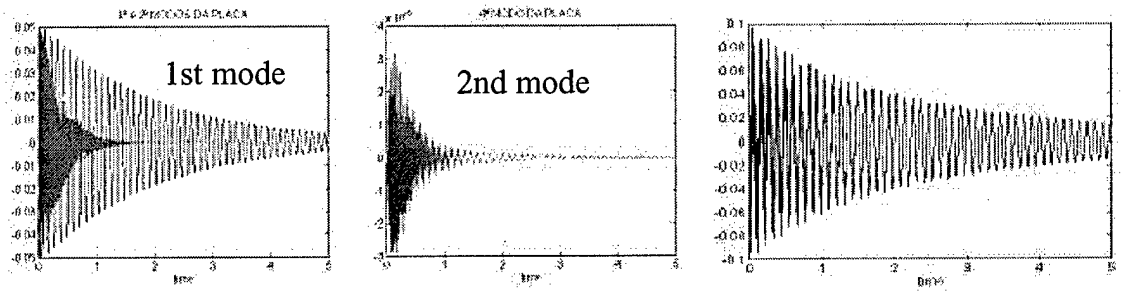

Figure 8 – Reduced order simulations showing that the first and second modes are controlled within 3 seconds and the time historu of the center plate vibration.

The passive control increases critical dynamic pressure by approximately 20% when setting the applied electric field to the maximum value (400 V). The effect of the piezoelectrically induced in-plane forces is small and it is concluded that passive control does not suppress flutter efficiently. The active control approach is attempted next, where the piezoelectric patches are assumed to impart only bending moments to the structure.

Thus, the optimal control theory was implemented to actively suppress flutter by using the piezoelectric patches to induce bending moments only. The panel deflection was represented by the first six modes. Nonlinear equations of motion have been used for all the numerical simulations. The maximum flutter free dynamic pressure λ_{max} is defined as the maximum λ under which the flutter can be completely suppressed with piezoelectric actuation. The numerical simulation showed that the flutter can be suppressed completely below λ_{max} by using the constant gain control feedback designed at the maximum dynamic pressure. The ration of λ_{max} to λ_{cr} was selected as an indicator for the performance or effectiveness of the piezoelectric actuator design.

The five configurations studied in the passive control methodology were considered for the active control methodology study. The results are presented below. It was observed that more piezoelectric actuators do not necessarily imply a better performance in active control approach as well. However, in the active control methodology, the performace is also dependent on the controller design. The active control method consistently performed better that the passive control methodology with 177% in aerodynamic pressure parameter as compared to 42% improvement in passive mode for configuration #1. The same trend was observed for other configurations. The results demonstrate that the bending actuation technique out-performs the passive control approach by an order of magnitude and that further simulations are necessary to study the effect of the controller design on the solution.

Critical Aerodynamic Parameter $\lambda_{cr} = 36.8$ (no piezoelectric patches)					
	#1	#2	#3	#4	#5
λ_{cr}	46.9	70.5	88.5	91.8	63.9
λ_{max}	128.6	163.4	152.5	175.5	115.8
$\frac{\lambda_{max}}{\lambda_{cr}}$	2.7	2.3	1.7	1.9	1.8

Concluding Remarks

A nonlinear supersonic flutter analysis of laminated composite plates and shells is carried out using a doubly curved quadrilateral thin shell finite element, developed on the basis of the Mindlin thin shell theory, classical lamination theory and linear piston aerodynamic theory. Numerical results are obtained for laminated composite plates and curved shells. The first-order piston theory used to model the aerodynamic pressure, provides a reasonable estimate of flutter, deflection shapes, and frequencies for thin plate/shell panels at approximate Mach numbers of greater than $\sqrt{2}$. Good agreement of the some of the obtained solutions with existing results served to establish the validity of the present formulation for supersonic flutter analysis of adaptive composite plates and shells.

The performance of flutter suppression using piezoelectric actuation is demonstrated by increasing the maximum flutter-free dynamic pressure λ_{max} or the ratio of the λ_{max} to the critical dynamic pressure λ_{cr}. The optimal control design is based on the linear equations of motion whereas the simulations are based on the nonlinear equations of motion. The numerical simulations show that the in-plane forces induced by the piezoelectric actuators are not very significant enough in order to considerably affect the flutter envelope. It was observed that the performace of the piezoelectric actuators in dynamic bending actuation mode is considerably superior compared to the passive actuation mode (177% improvement compared to 42% in the passive mode for configuration #1).

CHAPTER 5

EXPERIMENTAL BUFFET SUPPRESSION

Experimental buffeting and gust alleviation response results are presented for a sweptback flat wing model using piezoelectric actuators to control bending and wing tip camber shape. Model response was sensed by strain gages, accelerometers and piezoelectric sensors. The open-loop and closed-loop results of this experimental study show that piezoelectric actuation is effective in attenuating vibration and the wake-induced buffet response over the range of parameters investigated. The airfoil camber shape control increases remarkably the efficiency of the system, by using a controlled change of lift in order to produce the required bending moments.

Introduction

The primary passive solutions to dynamic aeroelastic problems consist of increasing the stiffness and blancing the mass and these have been used as early as 1922. They still comprise the basic passive means of improving the response and stability of an aircraft. Increased stiffness can also be achieved by using advanced composite tailoring which can greatly alter the stability characteristics of a given wing.

Active control concepts to improve the aeroelastic performance of wings have since emerged. The active aeroelastic control solutions consist of using aerodynamic control surfaces as they are readily available on conventional aircraft. One of the first active aeroelastic control experiments began testing in 1972 in NASA Langley Research Center's Transonic Dynamics Tunnel. The model was a clipped delta wing with a leading edge and a trailing edge actuator. Since that time, control experiments using flap actuators have studied a variety of control design techniques and objectives. The Active Flexible Wing project used the flexibility of the wing in conjunction with active controls to provide greater maneuverability.

In the last couple of decades, active aeroelastic control has evolved and a new actuation concept

has emerged for structural control. This is the direct strain actuation using adaptive materials and structures. These electro-magneto-thermo-mechanical materials have presented an exceptional promise when compared to conventional ones. For deformation of thin structural elements, the most widely used multifunctional materials are piezoelectric actuators. Piezoelectrics have several advantages over hydraulic actuators because they have a higher frequency bandwidth of operation and because they act directly in the structure by straining it. Piezoelectrics have higher bandwidths than are possible in shape memory alloys, they are more compact than magnetostrictive devices and they are bidirectional by nature unlike electrostrictive materials.

There has been considerable analytical and computational work performed to determine the feasibility of applying piezoelectric actuators to control wing flutter and buffeting. However, the experimental verification effort has been rather limited to a few studies reported in the literature. The DARPA/USAF Wright Laboratory program was to design, build and test wind tunnel models to quantify performance improvements that could be achieved by incorporating smart materials such has PZT's for actuation and sensing systems in aircraft wings. The Smart Wing program performed wind tunnel tests at the NASA Langley's Transonic Dynamic Tunnel to demonstrate the use of smart actuator systems in a realistic modeled aircraft operational environment. The wind tunnel test quantified aerodynamic improvements of two concepts: the use of embedded SMA wires in the trailing edge to provide a smooth variable contoured control surface, and SMA torque tubes built into the wing structure which enabled the wing to be twisted or torqued.

Several active vibrations suppression concepts have also been investigated by a program shared between Daimler-Benz Aerospace Military Aircraft (DASA), Daimler-Benz Forschung (DBF) and Deutsche Forchungsantalt fur Luftund Raumfahrt (DLR). Here, a thin surface of piezo actuators is set out to flatten the dynamic portion of the combined static and dynamic maximum bending moment loading case directly in the shell structure.

Crawley and de Luis [66] conducted one of the first studies on the use of piezoelectrics in vibration control of flexible structures. In the area of active buffet load alleviation, the first experiment demonstrating the feasibility of using piezoelectric actuators in aeroelastic control

was conducted by Heeg et al [67].

Shape control of a flexible wing structure has a great potential to improve the aerodynamic lifting-surface performance. Significant reductions in the shock-induced drag can be achieved by small adaptive modifications to the wing cross-sectional profile. The results presented here are the experimental wind tunnel results obtained to actively suppress buffeting by controlling the shape of the wing camber using piezoelectric actuators. Two methodologies are presented and compared. One uses the piezoelectric actuators in the traditional way, placing them at the root to generate bending moments to compensate the mechanical vibration along the span of the wing. The other method consists of using the piezoelectrics to achieve active airfoil camber shape control, in order to control lift, so that the change of lift can be used to generate the same type of moments and hopefully result in the use of fewer piezo actuators and less expended energy.

Experimental Model

The plate wing motion was controlled by six piezoceramic actuators bonded to the surface at the wing mount root portion and two shape control actuators near the wing tip. The piezo wafer sensors were located at the wing mount root and the signal was sent to digital signal processor through filters. The control signal was sent to power amplifiers. Amplified signal drove the piezoceramic actuators and attenuated vibration at the wing mount. This signal also drove the shape control actuators. A control law was designed based on a discrete system model.

A photograph and a sketch of the test model are shown in Figures 9, 10 and 11. The dimensions were determined based on the wind tunnel size, blowing air velocity and the limitations of the piezoceramic actuators. Structurally, it was aimed at having a fairly flexible wing with low bending and torsion mode frequencies.

Six piezoceramic sensor patches $38\times25\times0.2\ mm$ are adhered to the top and bottom of the plate near the root. The actuators (ACX-QPN40N) are divided in two groups, the ones that produce bending moments along the span of the wing, two pairs near the leading edge and one near the trailing edge, all near the root in order to maximise the bending moment. The other group, which

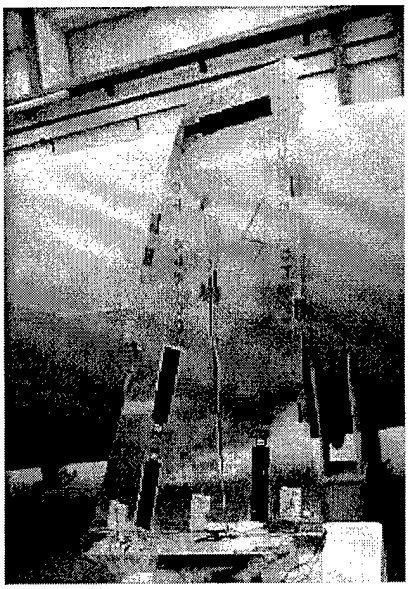

Figure 9. Wing with piezo actuators

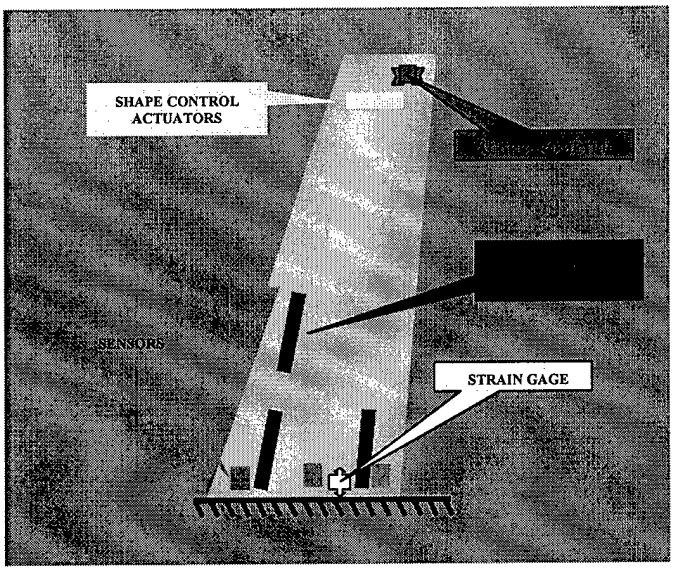

Figure 10. Wing with piezo actuators and sensors

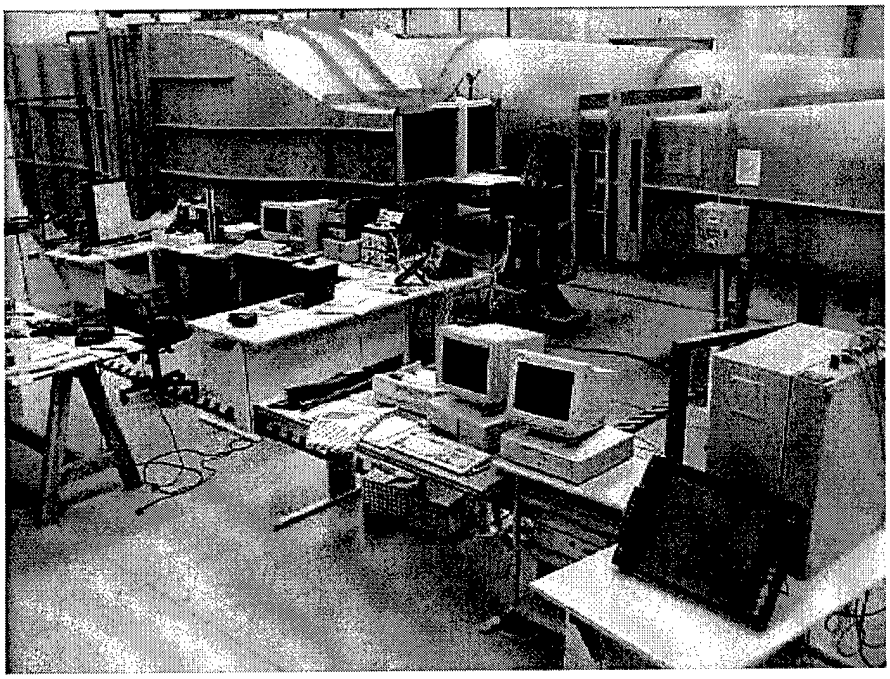

Figure 11. Wind tunnel test setup

is responsible for the camber shape control, is located near the wing tip in order to produce changes in the bending moment produced by the changes in lift. The output signal of the PZT sensors was made proportional to the vertical displacement of the model.

A finite element modal analysis was performed to generate natural frequencies and mode shapes needed to determine the appropriate placement of the piezoelectric actuating plates for maximum control authority and to design the controller. The vibration mode shapes and frequencies are shown in Figure 12.

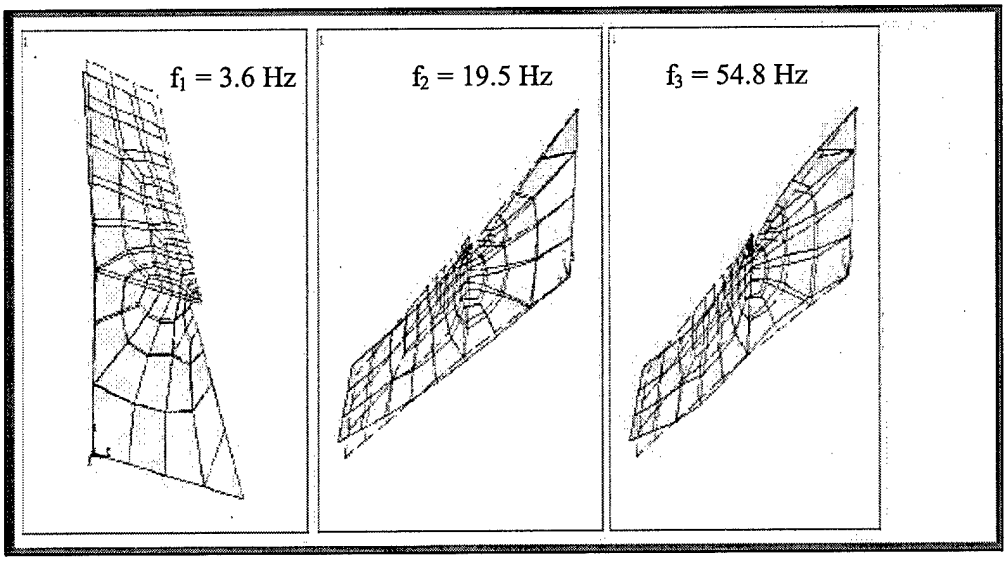

Figure 12. Wing Finite element model modal frequencies and mode shapes used in the controller design.

Controller Design

A block diagram of the controller feedback system is presented in Figure 13. The output analog signal from the PZT sensor mounted on the support root was routed to an analog-to-digital converter which had a sample rate of 10^{-4} seconds. The PZT sensor signal is proportional to and in phase with the displacement of the model. The digitized signal was then sent to the control law which was implemented on a MATLAB© and SIMULINK© environment running under a real time operating environment. The analog-to-digital converts were 32 bit units.

The control law was based on a simple feedback gain loop, i.e. the digital signal was multiplied by a constant value. The gained signal was next sent to a one step time delay. The time delay provides a means for changing the phase of the feedback signal. The gained- and phased-shifted signal was converted back to an analog signal by a zero-order-hold digital-to-analog converter. The converted signal was routed to two operational amplifiers. The output signals from the amplifiers were used to drive the piezoelectric actuators. The maximum output voltage from the amplifiers was +/- 100 volts. For the present study a sampling rate of 1000 samples per second was used. This relatively high rate was chosen to ensure that the buffeting waveform was well defined.

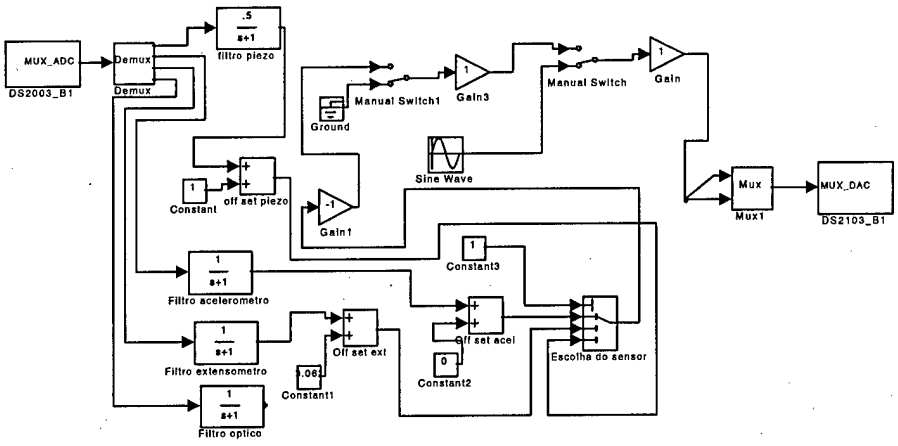

Figure 13. Schematic of the controller design MATLAB/SIMULINK ©

Test Results

The experimental set-up is based on a DSP state of the art laboratory facility created for testing and validating the theoretical models and application of active control methodologies. The objective of this test is to improve the damping characteristics of the structure and verify the method of analysis. The gain control method is used for the vibration control in the test being the following control law applied:

$$U = K_{gain}\, G_{filter}\, Y_{acc}$$

Were U is the Laplace transform of input u, K_{gain} is the multiplicative gain value, G_{filter} is a transfer function for low-pass filter, Y_{acc} is the Laplace transformation of the output y_{acc} of the sensor. The addition of the first-order low-pass filters enabled to improve the quality of the sensor signal.

Various sensor types were considered for application in the physical model. The sensors tested include a strain gage bridge, applied near the wing root where the structural loads are large; and an accelerometer, placed near the wing tip where the displacements are large. A good linearity in the response is required and it also important that the phase relationship between the various sensors is of good quality. In order to filter the low and high frequency contents of the response signals, they were subjected, at a later stage, to a low pass filtering with a cut off frequency of 50 Hz. In Figure 14, it can be seen a comparison of the signal coming from the different sensors, with and without filtering being applied, during forced vibration tests.

During the free vibration tests using the central root piezoelectric sensor, the time for the wing to stop oscillating after being forced to a 2 Hz regime was reduced from 40 seconds in open loop to 2 seconds when the loop was closed. In the same conditions, but using now the wing tip accelerometer as a sensor, the time for the wing to stop oscillating was reduced from 40 seconds in open loop to 4 seconds when the loop was closed.

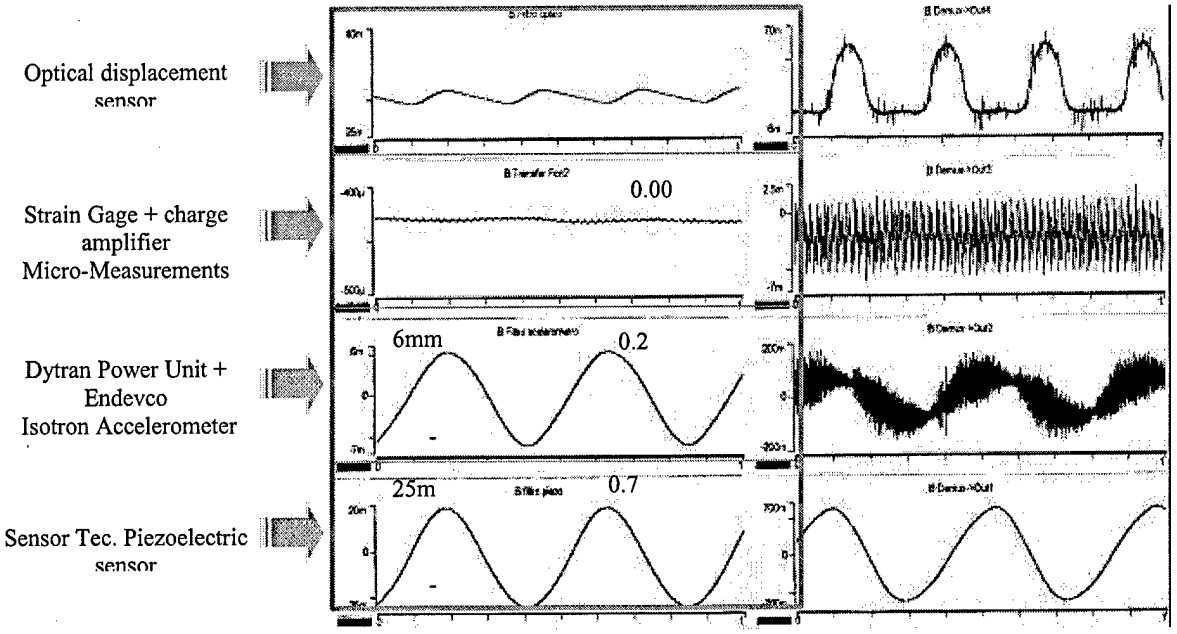

Figure 14. Sensor Identification

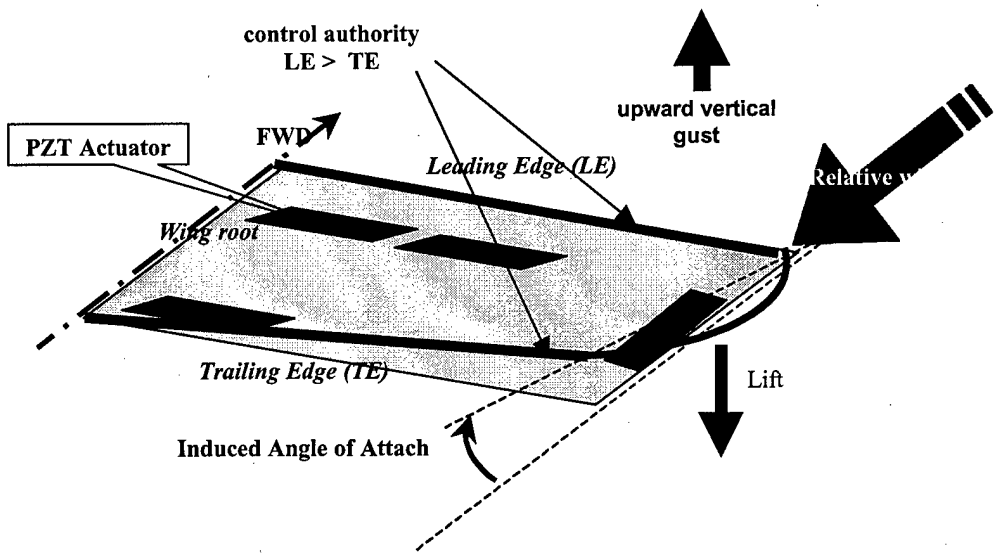

Figure 15. Wing reaction to an upward vertical gust

This simple test gave a good indication of the type of sensor to use, the amount of power required to achieve acceptable damping and the maximum amount of damping produced by the actuators and the control system. It can be inferred that the piezoelectric sensor presented the best quality in the measured signal.

The schematics for the buffet control test are the same as for the free vibration control test, the only difference, is that the wing panel was placed inside a wind tunnel. The system has a single output and a double input, one for the group of actuators that perform bending and another for the shape control (Figure 15).

For the present study the wind tunnel was modified so that a rigid plate was placed at the upstream end of the test section. The wake from this obstacle was used to generate buffeting flow. The position of this object could be easily adjusted so that the resulting wake would impinge on the model mounted downstream. The configuration finally selected was the one that produced the largest buffet response of the model. Therefore, all of the buffet response data presented herein were obtained for the obstacle in the same location and orientation. Tests were carried out with only the aluminium plate inside the wind tunnel, in order to determine the speeds at which the buffet would occur (a speed of 5.5 m/s was considered optimal).

With the control law gain set to the desired value the tunnel speed was increased to and then held constant at a pre selected value. Buffet response measurements were made at a velocity of 5.5 m/s. The output signal from the PZT sensor was channelled to a transfer function analyser that was used to calculate the auto-correlation function of the response signal. When the control laws are applied, the average amplitude due to buffeting decreased has it can be seen in Table 1.

Table1 - Experimental results

	Piezo damping		Piezo damping & shape control	
	Amplitude	Frequency	Amplitude	Frequency
Control law off	585 mm	1Hz	620 mm	1Hz
Control law on	395 mm	0.9 Hz	325 mm	0.66 Hz
Improvement	32 %	10%	47.5%	34%

An appreciable buffeting reduction has been obtained, especially when using airfoil shape control, which combined with the root actuators were able to decrease the average buffeting amplitude from 32% to 47.5%. The airfoil shape control also decreased the frequency of the vibration by 34%. The airfoil shape control has presented a feasible engineering design solution where the piezoelectric shape control actuators are used to create favorable changes in lift characteristics.

Preliminary Concluding Remarks

The concept and method of experimental aeroelastic vibration suppression using piezoceramic actuators and sensors to impart changes in damping and aerodynamic characteristics to the wing have been presented.

An appreciable buffeting reduction was obtained, especially when using airfoil shape control, which combined with the root actuators were able to decrease the average amplitude in buffeting from 32% to 47.5%. The airfoil shape control also decreased the frequency of the vibration by

34%. Future wind-tunnel test plans will focus on using a composite wing model as a testbed for active PZT sensing, actuation and shape control.

To resolve the diminishing control authority of the piezoceramic actuators as air speed is increased, the airfoil shape control has presented a feasible solution where the piezo actuators are used to create a favourable variation in lift characteristics.

CHAPTER 6

CONCLUSIONS AND FURTHER WORK

The adaptive structures design concepts proposed present engineering feasible solutions to problems requiring active vibration suppression and shape control in aircraft structures. The objective in adaptive composite structures is to have a structure that is capable of responding to the environment via control algorithms. Such structures would not only perform the functions programmed into it but also aim to maintain structural integrity and self-preservation.

The performance of flutter suppression using piezoelectric actuation is demonstrated by increasing the ratio of the λ_{max} to the critical dynamic pressure λ_{cr}. The optimal control design is based on the linear equations of motion whereas the simulations are based on the nonlinear equations of motion. The numerical simulations show that the in-plane forces induced by the piezoelectric actuators are not very significant enough in order to considerably affect the flutter envelope. It was observed that the performance of the piezoelectric actuators in dynamic bending actuation mode is considerably superior compared to the passive actuation mode (177% improvement compared to 42% in the passive mode).

The concept and method of experimental aeroelastic vibration suppression using piezoceramic actuators and sensors to impart changes in damping and aerodynamic characteristics to the wing have been presented. An appreciable buffeting reduction was obtained, especially when using airfoil shape control, which combined with the root actuators were able to decrease the average amplitude in buffeting from 32% to 47.5%. The airfoil shape control also decreased the frequency of the vibration by 34%. Future wind-tunnel test plans will focus on using a composite wing model as a testbed for active PZT sensing, actuation and shape control. To resolve the diminishing control authority of the piezoceramic actuators as air speed is increased, the airfoil shape control has presented a feasible solution where the piezo actuators are used to create a favourable variation in lift characteristics.

Further work is under way on two fronts: the first is to enhance the SMART STRUCTURES simulation program to carry out time domain simulations of the panel flutter phenomena and nonlinear control strategies such as feedback linearization technique are being incorporated for the active panel flutter control problem. On the experimental side, a more complex and three-dimensional model is being built to study the performance of the piezoelectric actuators and sensors in the wind-tunnel.

REFERENCES

1. G. Boyd and D.C. Lagoudas, Thermomechanical response of shape memory composites. J. Intell. Mater. Sys. Struct., 5, 333-346, (1993)
2. B.J. Sullivan, Analysis of properties of fiber composites with shape memory alloy constituents, Proceedings of the Second International Conference on Intelligent Materials, pp. 1194-1209, (1994)
3. C. Liang, and C.A. Rogers, One-dimensional thermomechanical constitutive relations for shape memory materials, J. Intell. Mater. Sys. Struct., 1, 207-234, (1990)
4. Z.C. Feng and D.Z. Li, Dynamics of a mechanical system with a shape memory alloy bar. J. Intell. Mater. Sys. Struct., 7, 399-410, (1996).
5. E.J. Graesser and F.A. Cozzarelli, A proposed three-dimensional constitutive model for shape memory alloys, J. Intell. Mater. Sys. Struct., 5, 78-89, (1994).
6. A. Baz, K. Iman and J. McCoy, Active vibration control of flexible beams using shape memory alloys. J. Sound and Vibration, 140, 437-456, (1990).
7. R. Ikegami, D.G. Wilson, J.R. Anderson and G. Julien, Active vibration control using nitinol and piezoelectric ceramics. J. Intell. Mater. Sys. Struct., 1, 189-206, (1990)
8. B.J. Maclean, G.J. Patterson and M.S. Misra, Modeling of a shape memory integrated actuator for vibration control of large space structures. J. Intell. Mater. Sys. Struct., 2, 72-94, (1990)
9. A.E. Clark, Giant magnetostriction materials from cryogenic temperatures at 250^0C. Proceedings of the SPIE, Vol. 1543, pp. 374-381, 1992.
10. T. Honda, K.I. Arai and M. Yamaguchi, Fabrication of actuators using magnetostrictive thin films, Proceedings of IEEE, Micro Electro-Mechanical Sys., Japan,, pp. 51-56,1994.

11. J. Bi and M. A. Anjanappa, Active vibration damping using magnetostrictive miniactuators, Smart Structures and Materials, N.W. Hagood (ed), SPIE Vol. 2190, pp. 171-181,1994.

12. A. Suleman and V.B. Venkayya, A simple finite element formulation for a laminated composite plate with piezoelectric layers, J. Intell. Mater. Sys. Struct., 6, 776-782 (1995).

13. T. Bailey and J.E. Hubbard, Distributed piezoelectric polymer active vibration control of cantilever beams, AIAA Journal, 25, 606-610 (1985).

14. E.F. Crawley and J. de Luis, Use of piezoelectric actuators as elements of intelligent structures, AIAA Journal, 25, 1373-1385, (1987).

15. M. Leibowitz and J.R. Vinson, Intelligent Composites, CCM Report 91-54, Center for Composite Materials, College of Engineering, University of Delaware, 1991.

16. B.T.Wang and C.A. Rogers, Laminate plate theory for spatially distributed induced strain actuators, Journal of Composite Materials, 25, 433-452 (1991).

17. C.L. Hom and N. Shankar, A fully coupled constitutive model for electrostrictive ceramic materials, J. Intell. Mater. Sys. Struct., 5, 795-801 (1994)

18. E. Prasad, The development of piezoelectric and electrostrictive sensors and actuators for incorporation into smart structures, Sensor Technology Ltd., CSA Stear-9 Report, 1997.

19. Y.C. Fung, On two dimensional panel flutter. Journal of the Astronautical Sciences, 25, 145-160(1958).

20. R.L. Bisplinghoff and H. Ashley, Principles of Aeroelasticity. Wiley, New York (1962)

21. E.H. Dowell, Panel flutter: a review of the aeroelastic stability of plates and shells. AIAA Journal, 8, 385-399(1970)

22. M.D. Olson, Some flutter solutions using finite elements. AIAA Journal, 8, 747-752 (1970)

23. G. Sander, C. Bon and M. Geradin, Finite element analysis of supersonic panel flutter. International Journal for Numerical Methods in Engineering, 7(3),379-394(1973)

24. T.Y. Yang and S.H. Sung, Finite element panel flutter in three-dimensional supersonic unsteady potential flow. AIAA Journal, 15(12), 1677-1683(1977).

25. C. Mei, A finite element approach for nonlinear panel flutter. AIAA Journal,15(8),1107-1110(1977)

26. R.M.V. Pidaparti and H.T Yang, Supersonic flutter analysis of composite plates and shells. AIAA Journal, 31(6), 1109-1117(1993).

27. J.N. Rosettos and P. Tong, Finite element analysis of vibration and flutter of cantilever anisotropic plates. American Society of Mechanical Engineers, paper 74-WA/APM-15 (1974).

28. R. S. Srinivasan and B.J.C. Babu, Free vibration and flutter of laminated quadrilateral plates. Journal of Computers and Structures, 27(2), 297-304(1987).

29. K.J. Lin, D.J. Lu and J.Q. Tarn, Flutter analysis of catilevered composite plates in subsonic flow. AIAA Journal, 27*8), 1102-1109(1989).

30. J.W. Sawyer, Flutter and buckling of general laminated plates. Journal of Aircraft, 14(4),387-393(1977).

31. G.A. Oyibo, Flutter of orthotropic panels in supersonic flow using affine transformations. AIAA Journal, 21(3), 282-289(1983).

32. I. Lee and M.H. Cho, Supersonic flutter analysis of clamped symmetric composite panels using shear deformable finite elements, AIAA Journal, 29(5), 782-783 (1991)

33. D.G. Liaw, Nonlinear supersonic flutter of laminated composite plates under thermal loads. Computers and Structures, 65(5),733-740(1997).

34. D.M. Lee and I. Lee, Vibration analysis of anisotropic plates with eccentric stiffener, Computers and Structures, 57, 99-105 (1995).

35. R.C. Zhou, Xue D.Y. and Mei C., Finite element time domain – modal formulation for nonlinear flutter of composite panels. AIAA Journal, 32(10), 2044-2052(1994).

36. K.S Rao and G. V. Rao, Large amplitude supersonic flutter of panels with ends elastically restrained against rotation. Computers and Structures, 11, 197-201(1980).

37. B.S. Sarma and T.K. Varadan, Nonlinear panel flutter by the finite element method. AIAA Journal, 26(5),566-574(1988).

38. C.E. Gray and C. Mei, Large amplitude finite element flutter analysis of composite panels in hypersonic flow, AIAA Journal, 31, 1090-1099 (1993)

39. C. Mei and D.J. Weidman, Nonlinear panel flutter – a finite element approach. ASME, New York, AMD-Vol. 26, 139-165(1977).

40. C. Mei and T.Y. Yang, Free vibrations of finite element plates subjected to complex middle-plane force systems. Journal of Sound and Vibration, 23(2),145-156(1972).

41. T.Y. Yang and A.D. Han, Flutter of thermally buckled finite element panels. AIAA Journal, 14,975-977(1976).

42. I.R. Dixon and C. Mei, Finite element analysis of large amplitude panel flutter of thin laminates. AIAA Journal, 31(4),701-107(1993)

43. D.G. Liaw and H.T.Y. Yang, Reliability and nonlinear supersonic flutter of uncertain laminated plates. AIAA Journal, 31(12),2304-2311(1993).

44. D.G. Liaw, Supersonic flutter of laminated thin plates with thermal effects, Journal of Aircraft, 30, 105-111 (1993)

45. D.Y. Xue and C. Mei, Finite element nonlinear panel flutter with arbitrary temperatures in supersonic flow. AIAA Journal, 31(1),154-162(1993).

46. R.C. Scott and T.A. Weisshaar, Controlling panel flutter using adaptive materials. Journal of Aircraft, 31, 213-222 (1994).

47. P. Hajela and R. Glowasky, Application fo piezoelectric elements in supersonic panels flutter suppression, AIAA Paper 91-2191 (1991).

48. R.C. Zhou, C. Mei and Huang J-K., Suppression of nonlinear panel flutter at supersonic speeds and elevated temperatures, AIAA Journal, 34(2),347-354(1996)

49. D.Y. Xue and C. Mei, A study of the application of shape memory alloys in panel flutter control. Proceedings of the 5th International Conference on Recent Advances in Structural Dynamics, 412-422 (1994).

50. H.S. Tzou and C.I. Tseng, Distributed piezoelectric sensor/actuator design for dynamic measurement/control of distributed parameter systems: A piezoelectric finite element approach, Journal of Sound and Vibration, 138, 17-34 (1990)

51. S.K. Ha, C. Keilers and F. Chang, Finite element analysis of composite structures containing distributed piezoceramic sensors and actuators, AIAA Journal, 30, 772-780 (1992).

52. C.K. Lee and F.C. Moon, Laminated piezopolymer plates for torsion and bending sensors and actuators, J. of the Acoustical Society of America, 85(6), 2432-2439 (1989).

53. E.F. Crawley and K.B. Lazarus, Induced strain actuation of isotropic and anisotropic plates, AIAA Journal, 29(6), 944-951 (1991).

54. B.T. Wang and C.A. Rogers., Laminated plate theory for spatially distributed induced strain actuators, Journal of Composite Materials, 25, 433-452 (1991).

55. K.Y. Lam, X.Q. Peng and J.N. Reddy, A finite element model for piezoelectric composite laminates, Smart Materials and Structures, 6, 583-591 (1997)

56. K. Chandrashekhara and A.N. Agarwal, Active control of laminated composite plates using piezoelectric devices: a finite element approach, J. Intell. Mater. Sys. Struct., 4, 496-508 (1993).

57. H.S. Tzou and R. Ye, Analysis of piezoelastic structures with laminated piezoelectric triangle shell elements, AIAA Journal, 34, 110-115 (1996).

58. C.C. Lin, C. Hsu and H. Huang, Finite element analysis on deflection control of plates with piezoelectric actuators, Composite Structures, 35, 423-433 (1996).

59. A. Chattopadhyay and C.E. Seeley, A higher order theory for modeling composite laminates with induced strain actuators, Composites, 28B, 243-252 (1997)

60. J.N. Reddy and J.A. Mitchell, Refined nonlinear theories of laminated composite structures with piezoelectric laminae, Journal of the Indian Academy of Sciences, 20, 721-747 (1995).

61. K.D. Jonnalagadda, T.R. Tauchert and G.E. Blandford, Higher-order displacement formulation for a piezothermoelastic laminate, Mechanics of Electromagnetic Materials and Structures, ASME, AMD-161/MD-42, 145-156 (1993).

62. R. Lammering, The application of a finite shell element for composites containing piezoelectric polymers in vibration control, Computers and Structures. 41, 1101-1109 (1991)

63. S.R. Thirupathi and N.G. Naganathan, A composite shell finite element for the analysis of smart structures, Smart Mater. Struct., SPIE Vol. 1916, 424-438, (1993).

64. V.V. Varadan, Y.H. Lim and V.K. Varadan, Closed loop finite element modeling of active/passive damping in structural vibration control, Smart Mater. Struct., 5, 685-694, (1996).

65. H.S. Tzou and R. Ye., Pyroelectric and thermal strain effects of piezoelectric devices. Adapt. Struct. Comp. Mater., ASME AD-45/MD-54, 125-132 (1994).

66. E.F. Crawley,. and J. de Luis, J., "Use of piezoelectric actuators as elements of intelligent structures", AIAA Journal, 25,1373-1385(1987)

67.. Heeg, J.M. Miller and R.V. Doggett, Attenuation of empennage buffet response through active ontrol of damping using piezoelectric material, NASA TM-107736(1993).